Comprehensive Multi-PTM Profiling Reveals Age-Associated Remodeling in Skeletal Muscle

Jian Li[1#], Xinqiang Lan[2#], Caifen Guo[3#], Xiang Wang[2#], Chunping Huang[2], Dongqin Zhang[4], Lin Zeng[5], Xiao-Li Tian[6*], Yang Xiang[2*] & Qiquan Wang[2*]

[1] Department of Sports Medicine, The Beijing Jishuitan Hospital Guizhou Hospital, Guiyang, China.

[2] Metabolic Control and Aging, Human Aging Research Institute and School of Life Science, Nanchang University, and Jiangxi Key Laboratory of Human Aging, Nanchang, China.

[3] Department of Urology, The Affiliated Hospital of Guizhou Medical University, Guiyang, China.

[4] HeartSeek Biotechnology, Kunming, China.

[5] Institutional Center for Shared Technologies and Facilities of the Kunming Institute of Zoology, Chinese Academy of Sciences, Kunming, China.

[6] Aging and Vascular Diseases, Human Aging Research Institute and School of Life Science, Nanchang University, and Jiangxi Key Laboratory of Aging and Diseases, Nanchang, China.

# These authors contribute equally to this work

*Corresponding author: Qiquan Wang, wangqiquan@ncu.edu.cn; Yang Xiang, xiangyang@ncu.edu.cn; Xiao-Li Tian, tianxiaoli@ncu.edu.cn;

Zoological Research

Abstract

Sarcopenia, characterized by the progressive loss of skeletal muscle mass and function, is a major hallmark of aging. Post-translational modifications (PTMs) play essential roles in regulating protein activity and cellular homeostasis; however, how multiple PTMs are remodeled during skeletal muscle aging remains incompletely characterized. Here, we performed comprehensive multi-layered proteomic profiling of skeletal muscle from young (3-month-old) and aged (24-month-old) mice, systematically quantifying the global proteome together with five major PTMs: acetylation, phosphorylation, N-glycosylation, O-glycosylation, and ubiquitination. In total, we identified 5,337 proteins and mapped thousands of PTM sites, generating an integrated atlas of age-associated proteomic and PTM remodeling in skeletal muscle. Pathway enrichment analyses revealed distinct modification-specific patterns: acetylation and phosphorylation were predominantly associated with metabolic and mitochondrial-related pathways; N-glycosylation was enriched in immune- and secretory pathway–related processes; O-glycosylation was associated with muscle contraction–related pathways; and ubiquitination was preferentially linked to cytoskeletal organization in muscle cells. Correlation analyses further uncovered diverse association patterns among different PTMs across protein- and modification-level datasets. Phosphorylation and ubiquitination exhibited consistent positive associations, whereas acetylation and ubiquitination showed both inverse and concordant co-variation patterns across subsets of proteins. Phosphorylation and O-glycosylation displayed heterogeneous association patterns across different proteins, and acetylation and phosphorylation demonstrated positive correlations with distinct age-associated directional changes across protein subsets. Together, these results provide a comprehensive, multi-dimensional view of age-associated remodeling of the skeletal muscle proteome and multiple PTM layers, offering a valuable resource for understanding molecular alterations accompanying muscle aging and sarcopenia.

Keywords: Sarcopenia, skeletal muscle aging, post-translational modification (PTM), acetylation, phosphorylation, glycosylation, ubiquitination

Introduction

Aging is characterized by a progressive decline in skeletal muscle mass, strength, and function, a clinical condition defined as sarcopenia (Cruz-Jentoft and Sayer, 2019). Sarcopenia severely impairs mobility, disrupts metabolic homeostasis, and substantially reduces quality of life among older individuals, representing a critical global health challenge as the proportion of the aging population rises (Petermann-Rocha et al., 2022; Shu et al., 2022). Consequently, there is an urgent need to elucidate the molecular mechanisms underlying skeletal muscle aging to develop effective interventions.

Advances in proteomics have significantly expanded our understanding of aging by revealing comprehensive proteome remodeling across various tissues, species, and life stages (Ding et al., 2025; Liu et al., 2025b; Moaddel et al., 2021; Reed et al., 2025; Wang et al., 2024; Yang et al., 2025). Recent quantitative proteomic studies in both human and rodent skeletal muscle have uncovered substantial age-related alterations in metabolic enzymes, structural and cytoskeletal proteins, and components involved in proteolysis (Doran et al., 2009; Murgia et al., 2017; Piec et al., 2005). However, alterations in protein abundance alone do not fully capture the regulatory complexity underlying functional decline during muscle aging.

Post-translational modifications (PTMs), including phosphorylation, acetylation, glycosylation, and ubiquitination, add an additional regulatory layer by modulating protein activity, localization, interactions, and stability (Mittal and Saluja, 2015; Wu et al., 2023; Zhong et al., 2023a). Increasing evidence indicates that age-associated changes in individual PTMs contribute to muscle dysfunction and metabolic imbalance

(Neal et al., 2024; Wei et al., 2018; Zhong et al., 2023b). Nevertheless, most studies to date have focused on single PTM types in isolation, leaving the broader landscape of PTM remodeling in aged skeletal muscle incompletely defined.

Distinct PTMs have been implicated in key aspects of skeletal muscle biology, including signaling, metabolism, proteostasis, and structural maintenance (Zhong et al., 2023b). Phosphorylation regulates major signaling pathways controlling muscle growth and metabolic homeostasis, such as mTORC1 (Saxton and Sabatini, 2017), AMPK (Kjøbsted et al., 2018), and insulin signaling (Gual et al., 2005). Lysine acetylation has been linked to mitochondrial function, metabolic enzyme regulation, proteostasis, and chromatin organization (Ito et al., 2002; Tian et al., 2020; Yoshihara et al., 2019). Glycosylation, particularly O-GlcNAcylation, is increasingly recognized as a nutrient-sensitive modification that integrates metabolic status with cellular stress responses and protein turnover in skeletal muscle (Blazev et al., 2021; Cieniewski-Bernard et al., 2004; Pélisse et al., 2018). Ubiquitination plays a central role in protein degradation via the ubiquitin–proteasome system and is a well-established driver of muscle atrophy through muscle-specific E3 ligases such as Atrogin-1 and MuRF1 (Bodine et al., 2001; Gomes et al., 2012; Sun-Wang et al., 2020). Despite these advances, how multiple PTMs are concurrently remodeled during skeletal muscle aging remains insufficiently characterized. Based on their well-established roles in skeletal muscle biology and aging, together with the availability of robust and quantitative enrichment workflows for large-scale proteomics, we focused in this study on five major PTM classes: phosphorylation, acetylation, ubiquitination, N-glycosylation, and O-glycosylation.

In this study, we performed a comprehensive, integrative proteomic analysis of skeletal muscle tissues from young (3-month-old) and aged (24-month-old) mice, the latter corresponding approximately to 70–80-year-old humans (Dutta and Sengupta, 2016). By combining high-resolution mass spectrometry with affinity-based enrichment strategies, we quantitatively profiled global protein abundance together with these five major PTM layers. This multi-layered approach enabled systematic characterization of

age-associated remodeling across the proteome and PTM landscapes. Our analyses provide an integrated atlas of protein- and PTM-level changes in aging skeletal muscle, offering a resource for future studies aimed at understanding molecular alterations associated with sarcopenia.

Results

Proteomic and PTM-omic profiling of young and aged skeletal muscle

To comprehensively characterize age-associated alterations in both the proteome and PTM landscape of skeletal muscle, we performed an integrative quantitative proteomic and PTM-omic analysis of quadriceps muscle harvested from young (3-month-old) and aged (24-month-old) mice **(Fig. 1A)**. Utilizing high-resolution mass spectrometry coupled with targeted affinity enrichment strategies, we confidently identified and quantified a total of 5,337 unique proteins. Among these proteins, we detected site-specific modifications involving 772 acetylated, 1,809 phosphorylated, 672 ubiquitinated, 220 N-glycosylated, and 156 O-glycosylated proteins, underscoring the diversity and abundance of PTM regulation in skeletal muscle **(Fig. 1B, Supplementary table 1)**.

Unsupervised hierarchical clustering of both global protein abundance data and PTM-specific profiles clearly distinguished aged samples from their young counterparts **(Fig. 1C)**. High reproducibility across biological replicates was further confirmed by strong sample–sample correlation at both the protein level and PTM site level **(Supplementary Fig. S1)**. Consistently, principal component analysis based on protein-level and PTM site–level quantification showed clear separation between young and aged samples without obvious outliers **(Supplementary Fig. S2)**. This distinct molecular signature indicates extensive and coordinated remodeling of protein expression alongside dynamic PTM alterations in aged skeletal muscle. Furthermore,

correlation analyses revealed a significant inverse association (adj. $P < 0.001$) between overall protein abundance changes and corresponding PTM modifications **(Fig. 1D)**, indicating that age-associated PTM remodeling is not merely driven by changes in protein expression levels. This inverse association highlights the importance of examining PTM regulation beyond protein abundance alone.

Global patterns of protein and PTM alterations in young and aged skeletal muscle

To characterize the molecular changes associated with aging, we systematically identified differentially expressed proteins and PTM-modified sites between young and aged skeletal muscle using stringent thresholds ($P < 0.05$; $|\log_2 FC| > 0.26$). Differential analyses at both the protein and PTM site levels were summarized using volcano plots to visualize effect size and statistical significance across all datasets **(Supplementary Fig. S3)**. Our analysis revealed 626 proteins significantly altered in abundance, accompanied by extensive remodeling across multiple PTM categories, including 827 acetylation sites (167 proteins), 1,246 phosphorylation sites (107 proteins), 172 ubiquitination sites (33 proteins), 227 N-glycosylation sites (15 proteins), and 58 O-glycosylation sites (7 proteins) **(Fig. 2A)**. Hierarchical clustering and heatmap visualization clearly differentiated young from aged muscle samples, underscoring pronounced and PTM-specific remodeling with age **(Fig. 2B)**.

To experimentally validate acetylation changes identified by the acetylome analysis, we performed immunoprecipitation–Western blot assays targeting myosin heavy chain (MyHC). Quadriceps muscle lysates from young and aged mice were pooled within each age group, followed by MyHC immunoprecipitation and immunoblotting with a pan–acetyl-lysine antibody. Consistent with the acetylome profiling results **(Supplementary table 1)**, aged skeletal muscle exhibited a reduction in overall MyHC acetylation compared with young controls **(Supplementary Fig. S4)**. These findings provide independent biochemical validation of the age-associated decline in MyHC acetylation detected by mass spectrometry–based analysis.

Pathway enrichment analysis using the KEGG database revealed distinct functional signatures across protein abundance and PTM-level changes during skeletal muscle aging **(Fig. 2C)**. Proteins exhibiting age-associated abundance changes were robustly enriched in pathways related to glutathione metabolism, cytoskeleton organization in muscle cells, and multiple cardiomyopathy-associated pathways, highlighting coordinated redox imbalance and structural remodeling as core features of aging skeletal muscle.

In contrast, PTM-level analyses demonstrated pronounced modification-specific enrichment patterns. Acetylation and phosphorylation changes were preferentially enriched in metabolic and mitochondrial-associated pathways, including oxidative phosphorylation and neurodegeneration-related modules, indicating extensive remodeling of energy metabolism and stress-responsive signaling at the post-translational level. Ubiquitination showed a more focused enrichment profile, with the strongest signal observed in the cytoskeleton in muscle cells pathway, suggesting selective ubiquitin-mediated regulation of muscle structural components and proteostasis during aging.

Glycosylation modifications displayed distinct and non-overlapping functional biases. N-linked glycosylation sites were significantly enriched in pathways related to complement and coagulation cascades, protein processing in the endoplasmic reticulum, and N-glycan biosynthesis, indicating prominent involvement of N-glycosylation in immune regulation and secretory pathway remodeling in aged muscle. In contrast, O-linked glycosylation exhibited significant enrichment specifically in the cardiac muscle contraction pathway, suggesting a more restricted association with contractile and excitation–contraction coupling processes.

Further Gene Ontology (GO) network analysis reinforced these functional distinctions, revealing clear PTM-specific clusters **(Fig. 2D)**. For instance, acetylation-associated GO terms centered on mitochondrial respiration and TCA cycle, whereas phosphorylation modifications grouped with muscle development and cellular stress

responses. Importantly, despite distinct functional enrichments, a strong positive correlation (adj. $P < 0.001$) was observed between KEGG pathway activity scores derived from the proteome and individual PTM datasets, calculated using z-score–based normalization **(Fig. 2E)**. This concordance at the pathway level indicates that proteomic and PTM alterations converge on overlapping biological processes, despite divergence at the individual protein or modification site levels.

Collectively, our data demonstrate that individual PTMs selectively regulate distinct functional modules, yet their coordinated interplay fundamentally contributes to the intricate molecular reprogramming underlying the aging skeletal muscle phenotype.

PTM-associated network during skeletal muscle aging

To define the association among diverse PTMs during skeletal muscle aging, we systematically analyzed overlaps between significantly altered proteins in the global proteome and PTM-specific datasets. In total, 57 proteins exhibited concurrent changes in both abundance and PTM status, indicating coordinated multi-layer regulation. In contrast, 559 proteins showed significant changes solely at the abundance level without detectable PTM modifications, whereas 252 proteins displayed PTM alterations independent of protein abundance shifts **(Fig. 3A, B)**. These results underscore distinct regulatory paradigms: some proteins undergo synchronized abundance and PTM modulation, while others are predominantly regulated by either PTMs or expression-level mechanisms.

Further examination revealed widespread patterns of PTM co-occurrence and site-level modification exclusivity in skeletal muscle. Specifically, 324 proteins were found to carry both acetylation and phosphorylation modifications, indicating frequent co-modification of these two PTM types. In addition, 319 proteins exhibited concurrent detection of phosphorylation and ubiquitination, consistent with previous reports describing the frequent association of these modifications within proteostasis-related pathways (Barbour et al., 2023). A smaller subset of proteins (26 proteins) displayed

both N-linked glycosylation and ubiquitination, suggesting a close association between glycan modification and protein turnover.

In contrast, only six instances of phosphorylation and O-glycosylation were detected at identical residues, indicating limited site-level overlap between these two PTMs. Notably, 812 lysine residues were observed to be modified by either acetylation or ubiquitination, reflecting extensive differential usage of lysine residues by acetylation and ubiquitination **(Fig. 3B)**.

Pathway enrichment analyses of PTM-defined protein subsets revealed distinct functional distributions across different regulatory categories during skeletal muscle aging **(Fig. 3C)**. Proteins exhibiting significant changes at both the proteome and PTM levels were predominantly enriched in pathways related to muscle contractile and structural function, including arrhythmogenic, hypertrophic, and dilated cardiomyopathies, reflecting the tight association between multilayer regulation and muscle integrity–related pathways during aging.

In contrast, proteins showing significant abundance changes in the absence of detectable PTM alterations were mainly enriched in pathways associated with cytoskeletal organization and antioxidant metabolism, including cytoskeleton in muscle cells and glutathione metabolism, indicating that expression-level regulation preferentially contributes to structural maintenance and redox homeostasis.

Proteins with unchanged global abundance but significant PTM alterations displayed a broader and more heterogeneous enrichment profile, spanning metabolic and signaling-related pathways, consistent with post-translational regulation acting as a flexible layer of functional modulation independent of protein abundance changes.

When further stratified by specific PTM co-occurrence patterns, proteins carrying both acetylation and ubiquitination were enriched in pathways related to cytoskeletal organization and metabolic processes, whereas proteins modified by both

phosphorylation and ubiquitination were preferentially associated with cytoskeleton-related and metabolic pathways, supporting coordinated regulation of structural and metabolic functions. Proteins carrying both N-linked glycosylation and ubiquitination showed enrichment in extracellular matrix–receptor interaction and cardiomyopathy-associated pathways, highlighting a potential role of N-glycosylation–linked proteostasis in muscle–ECM integrity.

In addition, proteins simultaneously modified by acetylation and phosphorylation were mainly enriched in central metabolic pathways, including glycolysis and pyruvate metabolism, underscoring coordinated regulation of energy metabolism. In contrast, proteins with phosphorylation and O-glycosylation detected at the same sites were relatively infrequent and exhibited limited pathway enrichment, primarily involving immune-related and muscle contraction–associated pathways, suggesting a more restricted and context-dependent regulatory role for this modification pair.

Together, these data illustrate distinct PTM-associated pathway patterns in skeletal muscle aging, reflecting multilayered molecular remodeling across protein abundance and modification states.

Proteomic network remodeling and functional clusters in skeletal muscle aging

To gain deeper insights into the functional relevance of age-associated proteomic changes in skeletal muscle, we analyzed the top 30 most significantly altered proteins ranked by fold change, representing the most robust abundance shifts associated with aging. These proteins predominantly mapped to metabolic pathways, cytoskeletal organization, and immune regulation **(Fig. 4A)**. Aging muscle displayed increased abundance of metabolic and lysosomal proteins such as cathepsin S (CTSS), lysosomal lipase A (LIPA), and insulin-like growth factor-binding protein 6 (IGFBP6). Conversely, proteins associated with anabolic growth and cellular proliferation, including the amino acid transporter SLC7A5 and DNA replication factor MCM6, exhibited marked downregulation. Collectively, these observations point to an aging-

induced proteomic shift toward enhanced catabolism and stress responses, alongside diminished anabolic capacity.

To explore how these proteomic changes were structurally organized, we constructed a protein–protein interaction (PPI) network from the set of differentially expressed proteins. Using density-based clustering analysis, we identified five distinct functional modules (Clusters 1–5) characterized by central hub proteins and enriched biological pathways **(Fig. 4B–E)**.

Cluster 1, centered around Caveolin-1 (CAV1), aminoadipate semialdehyde dehydrogenase (AASDH) and the fatty acid transporter CD36, was enriched in pathways involving muscle structural integrity, focal adhesion, and cardiomyopathies. Within this cluster, AASDH was notably downregulated, while CD36, CAV1, and adiponectin (ADIPOQ) showed pronounced upregulation, indicating coordinated remodeling of structural and metabolic pathways in aged muscle.

Cluster 2, featuring hub proteins hexose-6-phosphate dehydrogenase (H6PD), glucose-6-phosphate isomerase 1 (GPI1), and glutamine synthetase (GLUL), mapped strongly to metabolic pathways, including galactose metabolism, glutathione metabolism, and cofactor biosynthesis. Downregulation of glutamate–cysteine ligase catalytic subunit (GCLC), alongside upregulation of glutathione reductase (GSR), glutathione peroxidase 4 (GPX4), and glutathione peroxidase 7 (GPX7), reflected adaptive responses to oxidative stress in aging skeletal muscle.

Cluster 3 encompassed proteins involved in ribosome biogenesis and proteostasis, centered around ribosomal proteins such as ribosomal protein S20 (RPS20), ribosomal subunit L12 (RPL12), and ribosomal protein S29 (RPS29). The downregulation of these ribosomal proteins (such as RPS29, RPS20) suggested compromised protein synthesis capacity with advancing age.

Cluster 4, including albumin (ALB), plasminogen (PLG), and collagen type XVIII alpha 1 chain (COL18A1), was enriched in immune and systemic regulatory pathways, notably complement cascades, Fc gamma receptor–mediated phagocytosis, and endocytosis. Increased expression of ALB, antithrombin III (SERPINC1), clusterin (CLU), and PLG suggested age-related activation of inflammation-associated and extracellular transport–related processes.

Cluster 5 was characterized as a signaling-oriented module centered on CDP-diacylglycerol–inositol 3-phosphatidyltransferase (CDIPT), myotubularin 1 (MTM1), and inositol monophosphatase 1 (IMPA1), with significant enrichment in the phosphatidylinositol signaling system and inositol phosphate metabolism. Multiple enzymes involved in phosphoinositide synthesis and turnover—including CDIPT, MTM1, IMPA1, and phospholipase C delta 1 (PLCD1)—exhibited increased expression levels, indicating altered regulation of phosphoinositide-associated pathways during skeletal muscle aging.

Overall, this network-based analysis reveals that aging induces coordinated remodeling across interconnected proteomic modules, each reflecting distinct yet integrated biological adaptations associated with skeletal muscle aging and sarcopenia.

To further evaluate the translational relevance of the mouse model for human sarcopenia, we compared our mouse skeletal muscle proteome with a published human skeletal muscle aging dataset (PXD011967) (Ubaida-Mohien et al., 2019). Using Ensembl one-to-one ortholog mapping, we identified 70 aging-associated proteins that were consistently altered in both species **(Supplementary Fig. S5A)**.

Pathway enrichment analysis revealed that these conserved proteins were primarily enriched in muscle cytoskeleton organization and extracellular matrix–related pathways, including cytoskeleton in muscle cells, ECM–receptor interaction, and integrin signaling **(Supplementary Fig. S5B)**. Consistently, GO biological process analysis highlighted enrichment of terms related to muscle development, basement

membrane organization, and skeletal muscle regeneration **(Supplementary Fig. S5C)**, indicating that conserved aging-associated proteins between mouse and human predominantly contribute to the maintenance of muscle structural integrity and adaptive capacity during aging.

Patterns of phosphorylation and ubiquitination during skeletal muscle aging

To characterize the relationship between phosphorylation and ubiquitination in skeletal muscle, we examined correlations at the protein level across all modified proteins. A significant positive correlation was observed between phosphorylation and ubiquitination scores **(Fig. 5A)**, indicating coordinated variation of these two modifications across the skeletal muscle proteome.

Pathway-level analyses based on cumulative PTM intensities revealed distinct functional distributions for the two modifications **(Fig. 5B)**. Ubiquitination-associated changes were preferentially enriched in immune-related pathways, including graft-versus-host disease and T cell receptor signaling, whereas phosphorylation exhibited comparatively reduced enrichment in several classical signaling pathways, such as Wnt signaling and calcium signaling. These results suggest an age-associated redistribution of phosphorylation and ubiquitination across different functional domains rather than uniform changes across pathways.

Protein-level analyses further identified representative examples in which phosphorylation and ubiquitination levels were positively correlated across samples at the protein level **(Fig. 5C)**. Representative correlated protein pairs included laminin subunit gamma 1 (LAMC1) and voltage-dependent calcium channel gamma 6 subunit (CACNG6), microtubule affinity–regulating kinase 3 (MARK3) and tensin 1 (TNS1), alanine aminotransferase 2 (GPT) and guanine nucleotide-binding protein G(i) subunit alpha-3 (GNAI3), as well as ribosomal protein L3-like (RPL3L) and TNS1/GNAI3, illustrating concurrent variation of the two PTMs on proteins involved in related biological processes.

Comparative analyses between young and aged muscle further highlighted representative proteins exhibiting significant positive correlations between phosphorylation and ubiquitination across samples **(Fig. 5D)**. For several proteins, including Tropomyosin alpha-3 chain (TPM3), heat shock protein 90 alpha family class A member 1 (HSP90AA1), and vesicle-associated membrane protein 3 (VAMP3), aged muscle samples displayed a consistent shift toward higher phosphorylation and ubiquitination levels. These proteins are involved in cytoskeletal organization, metabolic processes, and proteostasis, reflecting protein-specific age-associated shifts in phosphorylation and ubiquitination levels.

Collectively, these results define context-dependent associations between phosphorylation and ubiquitination in aging skeletal muscle. The observed positive correlations highlight concurrent, protein-specific changes in these two PTMs across functional protein subsets.

Patterns of acetylation and ubiquitination at shared lysine residues during skeletal muscle aging

Lysine acetylation and ubiquitination both target the ε-amino group of lysine residues, allowing these modifications to occur at the same sites. Previous studies have reported that acetylation and ubiquitination can be associated at shared lysine residues, although the nature of this association may vary across different proteins and contexts (Caron et al., 2005; Li et al., 2012).

To characterize the relationship between acetylation and ubiquitination at the site level in skeletal muscle, we performed site-resolved analyses focusing on lysine residues annotated as carrying both modifications **(Fig. 6A)**. Correlation analyses revealed the presence of both negative and positive associations between acetylation and ubiquitination at individual lysine sites **(Fig. 6B)**.

Strong negative correlations were observed at multiple sites on structural and metabolic proteins, including titin (TTN K21921, K22087, K9407), tropomyosin alpha-1 chain (TPM1 K128, K248), glutamic-oxaloacetic transaminase 1 (GOT1 K290), and myozenin-1 (MYOZ1 K230) **(Fig. 6C)**. At these sites, acetylation levels were reduced whereas ubiquitination levels were relatively higher in aged muscle compared with young muscle **(Fig. 6D)**, indicating an inverse age-associated shift between the two modifications.

In contrast, several lysine sites exhibited positive correlations between acetylation and ubiquitination, including troponin I2, fast skeletal type (TNNI2 K99), myosin heavy chain 1 (MYH1 K273, K107, K730, K970), and sarcoplasmic/endoplasmic reticulum calcium ATPase 2 (ATP2A2 K757, K481, K128) **(Fig. 6C)**. For these sites, acetylation and ubiquitination levels varied in a concordant manner across samples. Notably, in aged muscle, many positively correlated sites showed lower relative levels of both modifications, highlighting coordinated but heterogeneous age-associated changes rather than uniform increases **(Fig. 6D)**.

Protein–protein interaction (PPI) network analyses further illustrated distinct organizational patterns between proteins belonging to the negative and positive correlation groups **(Fig. 6E)**. Proteins in the negatively correlated group formed clusters primarily comprising muscle contraction–related proteins together with proteins involved in stress-responsive ubiquitination and amino acid metabolic processes. In contrast, proteins from the positively correlated group displayed network clustering patterns that were more prominently linked to cytoskeletal components and energy metabolism–related proteins.

Consistent with these network-level patterns, KEGG pathway enrichment analysis revealed differential pathway associations between the two groups **(Fig. 6F)**. Negatively correlated proteins were preferentially enriched in pathways related to lipid and amino acid metabolic regulation, including PPAR signaling and ferroptosis. By contrast, positively correlated proteins were enriched in pathways associated with

central carbon metabolism and signaling-related processes, such as glycolysis/gluconeogenesis and longevity-related signaling pathways.

Representative examples of site-level co-variation patterns between acetylation and ubiquitination are shown in **Fig. 6G**. Metabolic and mitochondrial proteins, including acyl-CoA synthetase long-chain family member 1 (ACSL1 K428), malic enzyme 1 (ME1 K516), voltage-dependent anion channel 2 (VDAC2 K40), and glutamic-oxaloacetic transaminase 1 (GOT1 K290), exhibited negative correlations between acetylation and ubiquitination. In contrast, proteins involved in energy metabolism and calcium handling, such as phosphoglycerate mutase 2 (PGAM2 K61), sarcoplasmic/endoplasmic reticulum calcium ATPase 2 (ATP2A2 K757/K481), and phosphorylase kinase regulatory subunit beta (PHKB K40), showed positive correlations.

Collectively, these findings reveal distinct patterns of association between acetylation and ubiquitination in aging skeletal muscle, characterized by both inverse and concordant site-specific relationships across proteins involved in structural and metabolic processes.

Patterns of association between O-glycosylation and phosphorylation during skeletal muscle aging

To characterize the relationship between phosphorylation and O-glycosylation in skeletal muscle, we performed protein-level correlation analyses across all proteins detected with both modifications. A modest but statistically significant negative correlation was observed between phosphorylation and O-glycosylation (Pearson R ≈–0.11, adj.*P* = 0.047) **(Fig. 7A)**, suggesting an overall inverse association between these two PTMs at the proteome level.

Site-resolved analyses further revealed heterogeneous residue-specific association patterns **(Fig. 7B, C)**. At several sites, including ACTN3 S437 and MYH4 T1736,

phosphorylation levels were negatively correlated with O-glycosylation at the corresponding annotated residues. In contrast, positive correlations between phosphorylation and O-glycosylation were observed at other sites, such as CACNA2D1 S119, reflecting concordant variation of the two modifications at these positions.

Site-level heatmaps comparing young and aged muscle samples demonstrated age-associated directional shifts in both phosphorylation and O-glycosylation at these representative residues **(Fig. 7D)**. Together, these results highlight diverse, site-specific association patterns between O-glycosylation and phosphorylation in aging skeletal muscle, reflecting heterogeneous modes of co-variation across proteins and residues.

Patterns of association between acetylation and phosphorylation during skeletal muscle aging

To examine the association between acetylation and phosphorylation in skeletal muscle, we performed protein-level correlation analyses across proteins detected with both modifications. A significant positive correlation between acetylation and phosphorylation was observed at the proteome level **(Fig. 8A)**.

Proteins exhibiting statistically significant correlations spanned multiple functional categories, including metabolic enzymes such as lactate dehydrogenase A (LDHA) and aldolase C (ALDOC), cytoskeletal-associated proteins such as myosin-binding protein H (MYBPH) and myosin heavy chain 7 (MYH7), as well as molecular chaperones including heat shock protein family A member 5 (HSPA5) **(Fig. 8B)**. These results indicate that positive acetylation–phosphorylation associations occur across diverse protein classes in skeletal muscle.

Stratified analyses of proteins modified by both acetylation and phosphorylation revealed two distinct age-associated patterns **(Fig. 8C)**. A subset of proteins, including ribose-phosphate pyrophosphokinase 1 (PRPS1), HSPA5, TPM3, and heterogeneous nuclear ribonucleoprotein U (HNRNPU), displayed higher relative levels of both

acetylation and phosphorylation in aged muscle compared with young muscle. In contrast, proteins such as LDHA, myosin-binding protein H (MYBPH), glycogen phosphorylase (PYGM), and troponin T3 (TNNT3) exhibited lower relative levels of both modifications in aged muscle, indicating concordant age-associated decreases.

Based on these patterns, we further defined two groups of dual-modified proteins **(Fig. 8D)**. One group comprised proteins showing significant increased levels of both acetylation and phosphorylation in aged muscle (n = 2), including TPM3 and PRPS1. A second group included proteins exhibiting significant decreased levels of both PTMs (n = 5), such as ATL2, CACNA1S, YBX3, MYBPH, and HSPB6.

KEGG pathway enrichment analysis revealed distinct pathway association profiles for these two groups **(Fig. 8E)**. Proteins with increased acetylation and phosphorylation were enriched in pathways related to metabolic and muscle-associated processes, including purine metabolism, carbon metabolism, the pentose phosphate pathway, and cardiac muscle contraction–related pathways. Additional enrichment was observed in pathways linked to amino acid biosynthesis and hormone-responsive metabolic processes. In contrast, proteins showing decreased levels of both PTMs were enriched in pathways associated with neuroendocrine signaling and muscle contraction, including GnRH signaling, GABAergic synapse, aldosterone and cortisol synthesis, as well as cardiomyopathy-related pathways.

PPI network analyses further highlighted distinct network organization patterns for the two groups **(Fig. 8F, G)**. The dual-upregulated group formed networks primarily comprising proteins related to muscle-associated functions and nucleotide metabolism, whereas the dual-downregulated group displayed network clustering enriched in proteins involved in muscle structure, membrane trafficking and organelle dynamics, as well as RNA-binding and post-transcriptional regulation.

Collectively, these results delineate distinct age-associated patterns of concurrent acetylation and phosphorylation across protein subsets in skeletal muscle, accompanied

by divergent pathway enrichment and network organization profiles.

Discussion

Skeletal muscle aging is accompanied by complex molecular alterations that extend beyond changes in protein abundance, and PTMs provide a critical regulatory layer shaping protein function, stability, and cellular homeostasis (Zhong et al., 2023b). In this study, we performed integrated proteomic and PTM profiling to systematically quantify five major PTM classes—acetylation, phosphorylation, N-glycosylation, O-glycosylation, and ubiquitination—in young and aged mouse skeletal muscle. This dataset constitutes a comprehensive atlas of age-associated remodeling across both the proteome and multiple PTM layers, revealing modification-specific pathway distributions as well as protein- and site-level co-variation patterns that collectively define the molecular landscape of skeletal muscle aging.

At the proteome level, we quantified 5,337 proteins and identified 626 proteins exhibiting significant age-associated abundance changes. Pathway enrichment analysis consistently highlighted glutathione metabolism, cytoskeleton organization in muscle cells, and cardiomyopathy-related pathways as dominant features of aging skeletal muscle. These findings are highly consistent with prior large-scale proteomic studies in human skeletal muscle, which have linked aging to impaired redox regulation, structural remodeling, and altered proteostasis (Ubaida-Mohien et al., 2019). Importantly, by integrating publicly available human skeletal muscle aging datasets through ortholog mapping, we identified a subset of conserved aging-associated proteins enriched in cytoskeletal and extracellular matrix–related pathways. This cross-species concordance supports the translational relevance of the mouse model while also underscoring that species-specific regulatory components likely coexist with conserved molecular programs.

Beyond protein abundance, our integrated PTM profiling revealed pronounced modification-specific pathway distributions that would not be apparent from single-PTM or proteome-only analyses. Acetylation and phosphorylation changes preferentially mapped to metabolic and mitochondrial-associated pathways, including oxidative phosphorylation–linked modules, consistent with established roles of acetylation in regulating metabolic enzyme activity and mitochondrial function (Tian et al., 2020; Xiong and Guan, 2012), and of phosphorylation as a rapid and reversible regulator of cellular signaling and stress responses (Kjøbsted et al., 2018; Saxton and Sabatini, 2017). In contrast, ubiquitination exhibited a comparatively focused enrichment toward cytoskeleton-related pathways. This observation complements previous evidence linking ubiquitin–proteasome activity to muscle protein turnover and atrophy-related programs (Bodine et al., 2001; Gomes et al., 2012; Sun-Wang et al., 2020), while further suggesting that ubiquitination remodeling during aging may preferentially target specific structural networks rather than being uniformly distributed across the proteome.

Compared with phosphorylation, acetylation, and ubiquitination, glycosylation remodeling in skeletal muscle aging has remained less comprehensively characterized, particularly at the pathway level. In our dataset, N-glycosylation changes were significantly enriched in complement and coagulation cascades, protein processing in the endoplasmic reticulum, and N-glycan biosynthesis. This pattern aligns well with the established biology of N-glycosylation, which predominantly modifies secretory and membrane proteins and plays essential roles in protein folding, quality control, and immune-related signaling (Blazev et al., 2021; Reily et al., 2019). By contrast, O-glycosylation exhibited significant enrichment primarily in the muscle contraction pathway, indicating a more restricted pathway association in our current dataset. Given the relatively limited number of confidently quantified O-glycosylation sites compared with other PTM classes, this enrichment profile should be interpreted cautiously and may reflect selective detection of contractile or excitation–contraction coupling components rather than broad reprogramming of O-glycosylation across muscle

signaling systems—an issue that has also constrained prior large-scale analyses of O-glycosylation in skeletal muscle.

An important strength of multi-PTM profiling lies in its ability to examine co-variation and association patterns across distinct modification layers within the same biological context. Although our study is observational and does not establish direct mechanistic coupling, several association patterns identified here align closely with regulatory frameworks described in prior work. At the protein level, phosphorylation exhibited a consistent positive association with ubiquitination, in agreement with well-established models in which phosphorylation status correlates with ubiquitin-mediated protein turnover and proteostasis-related processes (Barbour et al., 2023; Hunter, 2007). Such coordinated variation suggests that phosphorylation and ubiquitination may act in concert during skeletal muscle aging to mark subsets of proteins undergoing enhanced remodeling or turnover.

Site-resolved analyses further revealed heterogeneous relationships between lysine acetylation and ubiquitination. Both inverse and concordant co-variation patterns were observed at shared lysine residues across structural and metabolic proteins, consistent with earlier reports that acetylation and ubiquitination can exhibit context-dependent occupancy and association across proteins and conditions (Caron et al., 2005; Li et al., 2012). Importantly, these site-level patterns were accompanied by distinct pathway enrichments: negatively associated sites were linked to lipid and amino acid metabolic regulation, including PPAR signaling and ferroptosis, whereas positively associated sites were associated with central carbon metabolism and longevity-related signaling pathways. These findings underscore the functional heterogeneity of acetylation–ubiquitination relationships in aging skeletal muscle.

We also identified previously underexplored associations between phosphorylation and O-glycosylation. While a modest inverse association was observed at the global proteome level, site-specific analyses revealed both negative and positive relationships at selected residues. This heterogeneity suggests that phosphorylation–O-glycosylation

associations are highly residue- and protein-dependent, potentially reflecting distinct regulatory states across contractile, cytoskeletal, and membrane-associated proteins in aging muscle.

In addition, acetylation and phosphorylation displayed a robust positive association at the protein level. Stratified analyses revealed subsets of proteins showing concordant increases or decreases in both modifications with age, spanning metabolic enzymes, cytoskeletal-associated proteins, and molecular chaperones. These coordinated patterns were accompanied by divergent pathway enrichment profiles, indicating that acetylation–phosphorylation co-variation reflects integrated regulatory responses across multiple functional modules rather than uniform directional changes across the proteome.

Collectively, these observations demonstrate that distinct PTM classes exhibit coordinated yet heterogeneous association patterns in aging skeletal muscle. By mapping these relationships across multiple PTM layers within the same biological samples, our study extends existing PTM regulatory frameworks into the context of muscle aging and highlights the value of integrated multi-PTM profiling for capturing layered molecular remodeling beyond single-modification analyses.

The integrated PTM changes observed here also suggest potential regulatory nodes that may be explored in future functional studies. If certain PTM alterations contribute to age-associated declines in muscle structure or function, targeted modulation of these modifications could represent a strategy to preserve muscle integrity. For example, α-actinin-3 (ACTN3), a protein linked to muscle performance (Berman and North, 2010), showed reduced acetylation and increased ubiquitination at specific lysine sites with age in our dataset. Although causal relationships cannot be inferred from the present analysis, this pattern is consistent with models in which acetylation status influences protein stability. Future studies examining whether maintaining ACTN3 acetylation—through modulation of acetyltransferases or deacetylases—can affect its turnover or muscle function would be of particular interest. Supporting this conceptual framework,

recent work has shown that promoting N-terminal acetylation can protect proteins from degradation and improve organismal fitness in model systems (Varland et al., 2023).

Despite providing extensive insights into age-associated PTM remodeling, several limitations merit consideration. First, this study examined only male mice, precluding assessment of sex-specific differences in skeletal muscle proteome and PTM regulation. Given well-documented sex-dependent differences in muscle aging trajectories, mitochondrial function, and metabolic regulation (De Jong et al., 2023; Kerr et al., 2024), future studies incorporating female cohorts will be essential to improve biological and translational relevance. Second, our analysis compared only two age points—young adulthood and advanced age—thereby focusing primarily on late-stage aging. Inclusion of intermediate age groups would help resolve the temporal progression of proteomic and PTM remodeling and distinguish early regulatory drivers from late-stage consequences of sarcopenia (Schaum et al., 2020). Third, although we observed substantial cross-species concordance at the proteome level, direct validation of PTM changes in human skeletal muscle will be necessary to establish translational relevance and clinical applicability.

In addition, this study focused on five major PTM classes with well-established relevance to skeletal muscle biology and aging—acetylation, phosphorylation, ubiquitination, N-glycosylation, and O-glycosylation—and did not include other biologically important modifications such as succinylation, crotonylation, or SUMOylation. Future studies incorporating a broader spectrum of PTMs will be required to achieve a more complete and integrative view of post-translational regulatory networks during skeletal muscle aging.

Finally, while we identified numerous correlations and co-variation patterns suggestive of PTM crosstalk, the present study is inherently observational and does not establish causal or temporal relationships among modifications. Targeted functional experiments, including genetic or pharmacological manipulation of specific PTM “writers” and “erasers” (such as kinases, acetyltransferases, deacetylases, or ubiquitin ligases), as

well as time-resolved analyses, will be essential to determine whether modulating specific PTMs can directly ameliorate age-related muscle dysfunction.

In summary, our integrative multi-PTM analysis provides a detailed, multi-dimensional atlas of post-translational remodeling in skeletal muscle aging, illustrating how coordinated networks of acetylation, phosphorylation, glycosylation, and ubiquitination regulate muscle metabolism, proteostasis, and structural integrity. These findings substantially advance understanding of the molecular mechanisms underlying sarcopenia and establish a valuable resource for future studies aimed at preserving muscle health during aging.

Materials and methods

Animal models and tissue collection

Male C57BL/6 mice were used in two age groups: young (3 months old) and aged (24 months old), with four mice per group. Skeletal muscle samples used for proteomic and PTM analyses were obtained exclusively from the quadriceps femoris muscle. This muscle group was selected due to its large size, mixed fiber-type composition, and its widespread use in studies of skeletal muscle aging.

Following euthanasia, mice were placed in the supine position, and the hindlimb skin was carefully removed. The quadriceps femoris muscle group, including the rectus femoris and vastus muscles, was exposed and dissected along natural fascial planes to avoid contamination from adjacent muscles such as the biceps femoris or sartorius. The muscle group was excised intact by severing its distal insertion at the patellar tendon and cutting its proximal attachments from the femur.

All dissections were performed using fine forceps and micro-dissection scissors by the same trained operator to minimize technical variability. Immediately after isolation,

muscle tissues were snap-frozen in liquid nitrogen and stored at −80°C until further processing. Identical dissection procedures were applied to all animals to ensure consistency across experimental groups. All procedures were approved by the Institutional Animal Care and Use Committee of Nanchang University (NCULAE-20221130019).

Protein extraction

Frozen quadriceps muscle tissues were individually ground into a fine powder under liquid nitrogen. The powdered samples were transferred into pre-cooled tubes and lysed in denaturing buffer containing 8 M urea, 100 mM triethylammonium bicarbonate (TEAB, pH 8.5), and 0.2% SDS. Samples were subjected to ultrasonication on ice for 5 min to ensure complete lysis and solubilization of proteins.

Cell debris was removed by centrifugation at 12,000 × g for 15 min at 4°C, and the supernatant was collected. Protein reduction was performed with 10 mM dithiothreitol (DTT) for 1 h at 56°C, followed by alkylation with iodoacetamide (IAM) for 1 h at room temperature in the dark. Proteins were precipitated by adding four volumes of pre-cooled acetone (−20°C) and incubating at −20°C for at least 2 h. The precipitated proteins were collected by centrifugation, washed twice with cold acetone, air-dried briefly, and re-dissolved in dissolution buffer containing 6 M urea and 100 mM TEAB (pH 8.5).

Protein concentrations were determined using the Bradford assay with bovine serum albumin (BSA) as a standard. Protein quality was further assessed by SDS–PAGE followed by Coomassie Brilliant Blue staining.

Protein digestion

For each sample, 10 mg of total protein was diluted with TEAB buffer and digested with sequencing-grade trypsin at an enzyme-to-substrate ratio of 1:50 (w/w) at 37°C for 4 h. An additional aliquot of trypsin was added and digestion was continued

overnight at 37°C. The reaction was terminated by acidification with formic acid to pH < 3. Digested peptides were centrifuged at 12,000 × g for 5 min, and the supernatant was desalted using C18 solid-phase extraction columns. After washing with 0.1% formic acid, peptides were eluted with 70% acetonitrile/0.1% formic acid and lyophilized to dryness.

Proteomics, DIA

Global proteome analysis was performed using a Vanquish™ Neo UHPLC system (Thermo Fisher Scientific, Germany) coupled to an Orbitrap Astral™ mass spectrometer (Thermo Fisher Scientific, Germany) operated in data-independent acquisition (DIA) mode. Lyophilized peptide samples were reconstituted in mobile phase A (0.1% formic acid in water), centrifuged at 14,000 × g for 20 min at 4°C, and 200 ng of peptide supernatant was injected for each analysis.

Peptides were first loaded onto a C18 trap column (5 mm × 300 μm, 5 μm particle size; Thermo Fisher Scientific) and subsequently separated on an analytical C18 column (PepMap™ Neo UHPLC, 150 μm × 15 cm, 2 μm particle size; Thermo Fisher Scientific) maintained at 50 °C. Mobile phase B consisted of 80% acetonitrile with 0.1% formic acid. Peptides were eluted using a linear gradient at a constant nanoLC flow rate.

The Orbitrap Astral mass spectrometer was equipped with an Easy-Spray™ electrospray ionization source operated at a spray voltage of 2.0 kV and an ion transfer tube temperature of 290°C. Full MS scans were acquired over an m/z range of 380–980 at a resolution of 240,000 (at m/z 200). DIA acquisition was performed using 300 isolation windows with a fixed window width of 2 Th. Fragment ions were acquired over an m/z range of 150–2000 at a resolution of 80,000, with a normalized collision energy (NCE) of 25% and a maximum injection time of 3 ms. All data were acquired in DIA mode and recorded as raw files (.raw).

Raw DIA data were processed using DIA-NN and Spectronaut software in library-free

(directDIA) mode. Spectra were searched against the *Mus musculus* UniProt Swiss-Prot reference proteome (release 2023_10_18). Search parameters included a precursor ion mass tolerance of 10 ppm and a fragment ion mass tolerance of 0.02 Da. Carbamidomethylation of cysteine was specified as a fixed modification, while oxidation of methionine was set as a variable modification. N-terminal modifications, including acetylation, methionine loss, and methionine loss followed by acetylation, were also considered. Trypsin was specified as the digestion enzyme, allowing up to two missed cleavage sites.

To ensure high-confidence identifications, peptide-spectrum matches (PSMs) were filtered to retain only those with confidence scores ≥99%. False discovery rate (FDR) control was applied at both peptide and protein levels using a target–decoy strategy, with an FDR threshold of 1%. Label-free protein quantification was performed based on precursor ion intensities generated by the DIA analysis pipeline. The resulting protein-level quantitative tables were used for downstream differential expression and pathway analyses.

Phosphoproteomics, DIA

Phosphorylated peptides were enriched using TiO_2 affinity chromatography according to the manufacturer's instructions. Briefly, lyophilized tryptic peptides were reconstituted in binding buffer and clarified by centrifugation. The supernatant was loaded onto TiO_2 columns pre-equilibrated with binding buffer and incubated at room temperature for 30 min to allow selective binding of phosphopeptides.

After incubation, the columns were centrifuged at 2,000 × g for 30 s and sequentially washed once with wash buffer and once with ultrapure water, each followed by centrifugation at 2,000 × g for 30 s. The collection tube was then replaced with a new, clean tube, and bound phosphopeptides were eluted using elution buffer. Eluted phosphopeptides were collected and lyophilized prior to LC–MS/MS analysis.

Phosphopeptides were analyzed using a Vanquish™ Neo UHPLC system (Thermo Fisher Scientific, Germany) coupled to an Orbitrap Astral™ mass spectrometer (Thermo Fisher Scientific, Germany) operated in data-independent acquisition (DIA) mode. Lyophilized phosphopeptides were dissolved in mobile phase A (0.1% formic acid in water), centrifuged at 14,000 × g for 20 min at 4°C, and 200 ng of peptide supernatant was injected for each analysis.

Peptides were separated on a C18 trap column (5 mm × 300 μm, 5 μm particle size; Thermo Fisher Scientific) followed by an analytical C18 column (PepMap™ Neo UHPLC, 150 μm × 15 cm, 2 μm particle size; Thermo Fisher Scientific) maintained at 50°C. Mobile phase A consisted of 0.1% formic acid in water, and mobile phase B consisted of 80% acetonitrile with 0.1% formic acid. Peptides were eluted using a linear gradient at a constant nanoLC flow rate.

The Orbitrap Astral mass spectrometer was equipped with an Easy-Spray™ electrospray ionization source operated at a spray voltage of 2.0 kV and an ion transfer tube temperature of 290°C. Full MS scans were acquired over an m/z range of 380–980 at a resolution of 240,000 (at m/z 200). DIA acquisition was performed using 300 variable isolation windows with a fixed window width of 2 Th. Fragment ions were acquired over an m/z range of 150–2000 at a resolution of 80,000, with a normalized collision energy (NCE) of 25% and a maximum injection time of 3 ms. All raw data were recorded in proprietary. raw format.

Raw DIA files were processed and analyzed using DIA-NN and Spectronaut software in library-free (directDIA) mode. Data were searched against the *Mus musculus* UniProt Swiss-Prot reference proteome (release 2023_10_18). The search parameters included a precursor mass tolerance of 10 ppm and a fragment mass tolerance of 0.02 Da. Carbamidomethylation of cysteine was set as a fixed modification, while oxidation of methionine was specified as a variable modification. N-terminal modifications, including acetylation, methionine loss, and methionine loss followed by acetylation, were also included. Trypsin was specified as the digestion enzyme, allowing up to two

missed cleavages.

To ensure high-confidence identifications, only peptide-spectrum matches (PSMs) with confidence scores ≥99% were retained. False discovery rate (FDR) control was applied at both peptide and protein levels using a target–decoy strategy, with an FDR threshold of 1%. Site-level phosphopeptide quantification tables generated by the software were used for downstream differential and correlation analyses.

Acetylomics, DDA

Lysine-acetylated peptides were enriched using anti–acetyl-lysine immunoaffinity beads (Cell Signaling Technology, USA) according to the manufacturer's protocol with minor modifications. Briefly, lyophilized tryptic peptides were dissolved in MOPS IAP buffer (50 mM MOPS, 10 mM KH_2PO_4, 50 mM NaCl) and clarified by centrifugation at 12,000 × g for 5 min at 4°C. The supernatants were incubated with anti–acetyl-lysine antibody–conjugated beads for 2 h at 4°C with gentle rotation.

After incubation, beads were pelleted by centrifugation (2,000 × g, 30 s, 4°C) and sequentially washed with pre-cooled MOPS IAP buffer followed by three washes with ultrapure water to remove nonspecifically bound peptides. Acetylated peptides were eluted twice with 0.15% trifluoroacetic acid (TFA) at room temperature for 10 min each. Eluates were combined, desalted using C18 StageTips, and lyophilized prior to LC–MS/MS analysis.

Enriched acetylated peptides were analyzed using an EASY-nLC™ 1200 UHPLC system (Thermo Fisher Scientific, Germany) coupled to a Q Exactive™ HF-X mass spectrometer (Thermo Fisher Scientific, Germany) operated in data-dependent acquisition (DDA) mode. Peptides were reconstituted in 0.1% formic acid (FA), centrifuged at 14,000 × g for 20 min at room temperature, and 1 μg of peptide solution was loaded onto a home-packed C18 nano-trap column (2 cm × 75 μm, 3 μm particle size), followed by separation on an analytical C18 column (15 cm × 150 μm, 1.9 μm

particle size). Mobile phase A consisted of water with 0.1% FA, and mobile phase B consisted of 80% acetonitrile with 0.1% FA. Peptides were eluted using a linear gradient at a constant flow rate suitable for nanoLC separation.

The Q Exactive HF-X mass spectrometer was operated with a Nanospray Flex™ ion source (spray voltage 2.3 kV; capillary temperature 320°C). Full MS scans were acquired in the Orbitrap over an m/z range of 350–1500 at a resolution of 120,000 (at m/z 200), with an automatic gain control (AGC) target of 3×10^6 and a maximum injection time of 80 ms. The top 30 most intense precursor ions were selected for higher-energy collisional dissociation (HCD) fragmentation. MS/MS spectra were acquired at a resolution of 15,000 (at m/z 200), with an AGC target of 5×10^4, a maximum injection time of 100 ms, and a normalized collision energy of 27%. Dynamic exclusion was enabled with a duration of 30 s to minimize repeated sequencing of abundant precursors.

Raw MS data files were processed using Proteome Discoverer (version 2.5, Thermo Fisher Scientific). Spectra were searched against the *Mus musculus* UniProt Swiss-Prot reference proteome (release 2023_10_18). Trypsin was specified as the proteolytic enzyme, allowing up to two missed cleavages. Carbamidomethylation of cysteine was set as a fixed modification. Oxidation of methionine and acetylation of lysine were specified as variable modifications. N-terminal acetylation, methionine loss, and methionine loss followed by acetylation were also included as variable N-terminal modifications.

Precursor ion mass tolerance was set to 10 ppm, and fragment ion mass tolerance was set to 0.02 Da. Peptide-spectrum matches (PSMs) were filtered using a false discovery rate (FDR) of 1% at both the peptide and protein levels, based on a target–decoy strategy. Proteins identified with at least one unique peptide were considered confidently identified. Label-free quantification was performed using precursor ion intensities extracted by Proteome Discoverer.

Ubiquitylomics, DDA

Ubiquitin remnant–containing peptides (K-ε-GG) were enriched using the PTMScan® Ubiquitin Remnant Motif Kit (Cell Signaling Technology) according to the manufacturer's instructions. Briefly, lyophilized tryptic peptides were resuspended in MOPS IAP buffer (50 mM MOPS, 10 mM KH_2PO_4, 50 mM NaCl) and clarified by centrifugation at 12,000 × g for 5 min. The supernatants were incubated with anti–K-ε-GG antibody–conjugated beads at 4°C for 2 h with gentle rotation. After incubation, the beads were washed sequentially with pre-cooled MOPS IAP buffer and water to remove non-specifically bound peptides. Ubiquitinated peptides were eluted twice using 0.15% trifluoroacetic acid (TFA), and the combined eluates were desalted and lyophilized.

For LC–MS/MS analysis, peptides were reconstituted in 0.1% formic acid and analyzed using an EASY-nLC™ 1200 UHPLC system (Thermo Fisher Scientific) coupled to a Q Exactive™ HF-X mass spectrometer (Thermo Fisher Scientific) operated in data-dependent acquisition (DDA) mode. Peptides were loaded onto a homemade C18 trap column (2 cm × 75 μm, 3 μm) and separated on a homemade analytical column (15 cm × 150 μm, 1.9 μm). The mass spectrometer was operated with a nanospray voltage of 2.3 kV and a capillary temperature of 320°C. Full MS scans were acquired over an m/z range of 350–1500 at a resolution of 120,000 (m/z 200), with an AGC target of 3×10^6 and a maximum injection time of 80 ms. The top 30 most abundant precursor ions were selected for higher-energy collisional dissociation (HCD) with a normalized collision energy of 27% and analyzed at a resolution of 15,000 (m/z 200). Dynamic exclusion was set to 30 s.

Raw MS data were processed using Proteome Discoverer version 2.5 (Thermo Fisher Scientific) and searched against the Mus musculus UniProt Swiss-Prot reference proteome (release 2023_10_18). Trypsin was specified as the digestion enzyme with up to two missed cleavages allowed. Carbamidomethylation of cysteine was set as a fixed modification, while oxidation of methionine and diglycine modification of lysine

(K-ε-GG) were specified as variable modifications. Precursor and fragment ion mass tolerances were set to 10 ppm and 0.02 Da, respectively. Peptide-spectrum matches (PSMs) and proteins were filtered at a 1% false discovery rate (FDR) at both peptide and protein levels. Proteins identified by at least one unique peptide were retained for downstream analyses. Label-free quantification was performed based on precursor ion intensities.

Glycomics, DDA

Glycopeptides were enriched using hydrophilic interaction liquid chromatography (HILIC). Briefly, tryptic peptides were dissolved in 80% acetonitrile containing 0.1% trifluoroacetic acid (TFA) and incubated under HILIC conditions to selectively retain glycopeptides. The enriched fractions were washed sequentially with 0.5% TFA (three times) and 5% acetonitrile containing 0.5% TFA (once) to remove non-specifically bound peptides. Glycopeptides were then eluted and lyophilized prior to LC–MS/MS analysis.

UHPLC–MS/MS analyses were performed using an EASY-nLC™ 1200 UHPLC system (Thermo Fisher Scientific, Germany) coupled to a Q Exactive™ HF-X mass spectrometer (Thermo Fisher Scientific, Germany), operated in data-dependent acquisition (DDA) mode. Full MS scans were acquired in the Orbitrap over an m/z range of 300–1400 at a resolution of 120,000 (at m/z 200), with a maximum injection time of 50 ms. MS/MS spectra were acquired at a resolution of 15,000 (at m/z 200) with a maximum injection time of 22 ms, using higher-energy collisional dissociation (HCD) with a normalized collision energy of 35%. Dynamic exclusion was enabled with an exclusion duration of 18 s. Mobile phase A consisted of 0.1% formic acid in water, and mobile phase B consisted of acetonitrile containing 0.1% formic acid.

Raw MS data were searched using pGlyco 3.0 against *Mus musculus* UniProt Swiss-Prot reference proteome (release 2023_10_18) using distinct N-glycan and O-glycan databases, respectively, to distinguish N-linked and O-linked glycopeptides. Search

parameters included a precursor ion mass tolerance of 10 ppm and a fragment ion mass tolerance of 20 ppm. Carbamidomethylation of cysteine was specified as a fixed modification, while oxidation of methionine and N-terminal acetylation were set as variable modifications. Trypsin was specified as the digestion enzyme, allowing up to two missed cleavages.

Search results were imported into pGlycoQuant for glycopeptide-level quantitative analysis. Glycopeptide-spectrum matches (PSMs) were filtered using a 1% false discovery rate (FDR) threshold, and only PSMs with confidence values ≥99% were retained. Proteins supported by at least one unique glycopeptide were considered confidently identified, with FDR controlled at <1% at both peptide and protein levels. Due to the intrinsic limitations of HCD-based fragmentation, glycosylation analyses were interpreted primarily at the peptide and protein levels rather than relying on unambiguous residue-level site localization.

Bioinformatics and statistical analysis

Multi-omics data were organized and analyzed using a standardized workflow to ensure consistent integration, normalization, and reproducibility (Liu et al., 2025a). To correct PTM site-level quantification for protein abundance effects, PTM intensities were normalized against the corresponding protein-level intensities derived from the global proteome dataset. For each matched PTM–protein pair, normalized PTM values were calculated as the ratio of PTM site intensity to the corresponding protein intensity within the same sample. These protein-adjusted PTM values were subsequently used for downstream analyses.

For differential expression analyses between young and aged groups, independent two-sample *t* tests were applied at the protein and PTM site levels. Nominal *P* values were retained for downstream exploratory analyses to avoid overly conservative filtering and to preserve potentially informative features for pathway- and correlation-based analyses. Identified proteins and modification sites were considered significantly changed between young and aged groups if they met the criteria of $P < 0.05$ and |log2

fold change| > 0.26.

For pathway enrichment analyses (KEGG and Gene Ontology), Benjamini–Hochberg false discovery rate (BH-FDR) correction was applied in all analyses, and adjusted *P* values (q values, adj.*P*) were used for visualization in all enrichment-related figures. Except for one KEGG enrichment subfigure used solely for candidate pathway prioritization, all enrichment results were visualized without hard filtering by nominal *P* values or FDR-adjusted q values, allowing comprehensive inspection of pathway-level trends. Functional annotation of proteins was performed using InterProScan, Clusters of Orthologous Genes (COG), and KEGG pathway analysis. Differentially expressed proteins were subjected to KEGG pathway enrichment analysis using the clusterProfiler package in R (Yu et al., 2012). Gene Ontology (GO) enrichment analysis and network visualization of enriched terms were carried out with Metascape (Zhou et al., 2019) Protein-protein interaction (PPI) networks for selected protein sets were constructed using the STRING database (Franceschini et al., 2013) and visualized in Cytoscape (Shannon et al., 2003). Hierarchical clustering heatmaps for differentially expressed proteins and modified sites were generated with the pheatmap R package (v1.0.12) to visualize expression patterns.

Correlation analyses between different PTM datasets or between protein and PTM levels were performed and visualized using the corrplot R package (v0.92). Correlation analyses between protein abundance and PTM site intensities, as well as between different PTM datasets, were performed using Pearson correlation coefficients. Each correlation analysis was based on four biological replicates per group. Corresponding *P* values were adjusted using the Benjamini–Hochberg FDR correction to generate adjusted *P* values (adj.*P*, q values). In selected figures, both nominal *P* values and FDR-adjusted *P* values were reported to allow transparent evaluation of correlation trends, particularly in cases where adj.*P* values did not reach statistical significance. Additional data visualizations (bar graphs, scatter plots, lollipop charts, Venn diagrams, boxplots) were created using ggplot2 (v3.5.0) and related R packages such as ggVennDiagram

v1.5.2 for Venn diagrams. Pathway activity scores (Z-scores) for proteomic and PTM data were calculated to compare relative pathway perturbations; Z-scores were computed in Python (v3.11) using SciPy (v1.13.0) (Elam et al., 2019).

Immunoprecipitation and Western blot analysis

To validate age-associated changes in MyHC acetylation, immunoprecipitation–Western blot assays were performed using skeletal muscle samples from young and aged mice. Quadriceps muscles were collected from young (3-month-old, n = 4) and aged (24-month-old, n = 4) male C57BL/6 mice. For each age group, equal amounts of muscle tissue were pooled to minimize inter-individual variability and to obtain sufficient protein material for immunoprecipitation.

Muscle tissues were homogenized in ice-cold lysis buffer containing protease inhibitors. Lysates were clarified by centrifugation, and equal amounts of total protein were subjected to immunoprecipitation using an anti-MyHC antibody (DSHB) overnight at 4°C with gentle rotation. Immune complexes were captured using protein A agarose beads, washed extensively, and eluted in SDS sample buffer.

Immunoprecipitated proteins were separated by SDS–PAGE and transferred to PVDF membranes. Membranes were probed with a pan–acetyl-lysine antibody (PTM Bio) to assess overall acetylation levels of MyHC, followed by reprobing with anti-MyHC antibody to confirm equal immunoprecipitation efficiency. Signals were visualized using enhanced chemiluminescence and quantified by densitometry.

References

Barbour H, Nkwe NS, Estavoyer B, et al. 2023. An inventory of crosstalk between ubiquitination and other post-translational modifications in orchestrating cellular processes. *iScience*, **26**(5): 106276.

Berman Y & North KN. 2010. A gene for speed: the emerging role of alpha-actinin-3 in muscle metabolism. *Physiology (Bethesda)*, **25**(4): 250-259.

Blazev R, Ashwood C, Abrahams JL, et al. 2021. Integrated Glycoproteomics Identifies a Role of N-Glycosylation and Galectin-1 on Myogenesis and Muscle Development. *Mol Cell Proteomics*, **20**: 100030.

Bodine SC, Latres E, Baumhueter S, et al. 2001. Identification of ubiquitin ligases required for skeletal muscle atrophy. *Science*, **294**(5547): 1704-1708.

Caron C, Boyault C, Khochbin S. 2005. Regulatory cross-talk between lysine acetylation and ubiquitination: role in the control of protein stability. *Bioessays*, **27**(4): 408-415.

Cieniewski-Bernard C, Bastide B, Lefebvre T, et al. 2004. Identification of O-linked N-acetylglucosamine proteins in rat skeletal muscle using two-dimensional gel electrophoresis and mass spectrometry. *Mol Cell Proteomics*, **3**(6): 577-585.

Cruz-Jentoft AJ & Sayer AA. 2019. Sarcopenia. *Lancet*, **393**(10191): 2636-2646.

De Jong J, Attema BJ, Van Der Hoek MD, et al. 2023. Sex differences in skeletal muscle-aging trajectory: same processes, but with a different ranking. *Geroscience*, **45**(4): 2367-2386.

Ding Y, Zuo Y, Zhang B, et al. 2025. Comprehensive human proteome profiles across a 50-year lifespan reveal aging trajectories and signatures. *Cell*, **188**(20): 5763-5784.e5726.

Doran P, Donoghue P, O'connell K, et al. 2009. Proteomics of skeletal muscle aging. *Proteomics*, **9**(4): 989-1003.

Dutta S & Sengupta P. 2016. Men and mice: Relating their ages. *Life Sci*, **152**: 244-248.

Elam KK, Clifford S, Shaw DS, et al. 2019. Gene set enrichment analysis to create polygenic scores: a developmental examination of aggression. *Transl Psychiatry*, **9**(1): 212.

Franceschini A, Szklarczyk D, Frankild S, et al. 2013. STRING v9.1: protein-protein interaction networks, with increased coverage and integration. *Nucleic Acids Res*, **41**(Database issue): D808-815.

Gomes AV, Waddell DS, Siu R, et al. 2012. Upregulation of proteasome activity in muscle RING finger 1-null mice following denervation. *Faseb j*, **26**(7): 2986-2999.

Gual P, Le Marchand-Brustel Y, Tanti JF. 2005. Positive and negative regulation of insulin signaling through IRS-1 phosphorylation. *Biochimie*, **87**(1): 99-109.

Hunter T. 2007. The age of crosstalk: phosphorylation, ubiquitination, and beyond. *Mol Cell*, **28**(5): 730-738.

Ito A, Kawaguchi Y, Lai CH, et al. 2002. MDM2-HDAC1-mediated deacetylation of p53 is required for its degradation. *Embo j*, **21**(22): 6236-6245.

Kerr HL, Krumm K, Anderson B, et al. 2024. Mouse sarcopenia model reveals sex- and age-specific differences in phenotypic and molecular characteristics. *J Clin Invest*, **134**(16).

Kjøbsted R, Hingst JR, Fentz J, et al. 2018. AMPK in skeletal muscle function and metabolism. *Faseb j*, **32**(4): 1741-1777.

Li H, Wittwer T, Weber A, et al. 2012. Regulation of NF-κB activity by competition between RelA acetylation and ubiquitination. *Oncogene*, **31**(5): 611-623.

Liu B, Liu Y, Xu S, et al. 2025a. EasyMultiProfiler: an efficient multi-omics data integration and analysis workflow for microbiome research. *SCIENCE CHINA Life Sciences*.

Liu WS, You J, Chen SD, et al. 2025b. Plasma proteomics identify biomarkers and undulating changes of brain aging. *Nat Aging*, **5**(1): 99-112.

Mittal S & Saluja D. 2015. Protein post-translational modifications: role in protein structure, function and stability. *In*. Proteostasis and chaperone surveillance. Springer, 25-37.

Moaddel R, Ubaida-Mohien C, Tanaka T, et al. 2021. Proteomics in aging research: A roadmap to clinical, translational research. *Aging Cell*, **20**(4): e13325.

Murgia M, Toniolo L, Nagaraj N, et al. 2017. Single Muscle Fiber Proteomics Reveals Fiber-Type-Specific Features of Human Muscle Aging. *Cell Rep*, **19**(11): 2396-2409.

Neal CL, Kronert WA, Camillo JRT, et al. 2024. Aging-affiliated post-translational modifications of skeletal muscle myosin affect biochemical properties, myofibril

structure, muscle function, and proteostasis. *Aging Cell*, **23**(6): e14134.

Pélisse M, Der Vartanian A, Germot A, Maftah A. 2018. Protein O-Glucosyltransferase 1 Expression Influences Formation of Differentiated Myotubes in C2C12 Cell Line. *DNA Cell Biol*, **37**(4): 359-372.

Petermann-Rocha F, Balntzi V, Gray SR, et al. 2022. Global prevalence of sarcopenia and severe sarcopenia: a systematic review and meta-analysis. *J Cachexia Sarcopenia Muscle*, **13**(1): 86-99.

Piec I, Listrat A, Alliot J, et al. 2005. Differential proteome analysis of aging in rat skeletal muscle. *Faseb j*, **19**(9): 1143-1145.

Reed ER, Chandler KB, Lopez P, et al. 2025. Cross-platform proteomics signatures of extreme old age. *Geroscience*, **47**(1): 1199-1220.

Reily C, Stewart TJ, Renfrow MB, Novak J. 2019. Glycosylation in health and disease. *Nat Rev Nephrol*, **15**(6): 346-366.

Saxton RA & Sabatini DM. 2017. mTOR Signaling in Growth, Metabolism, and Disease. *Cell*, **168**(6): 960-976.

Schaum N, Lehallier B, Hahn O, et al. 2020. Ageing hallmarks exhibit organ-specific temporal signatures. *Nature*, **583**(7817): 596-602.

Shannon P, Markiel A, Ozier O, et al. 2003. Cytoscape: a software environment for integrated models of biomolecular interaction networks. *Genome Res*, **13**(11): 2498-2504.

Shu X, Lin T, Wang H, et al. 2022. Diagnosis, prevalence, and mortality of sarcopenia in dialysis patients: a systematic review and meta-analysis. *J Cachexia Sarcopenia Muscle*, **13**(1): 145-158.

Sun-Wang JL, Ivanova S, Zorzano A. 2020. The dialogue between the ubiquitin-proteasome system and autophagy: Implications in ageing. *Ageing Res Rev*, **64**: 101203.

Tian H, Liu S, Ren J, et al. 2020. Role of Histone Deacetylases in Skeletal Muscle Physiology and Systemic Energy Homeostasis: Implications for Metabolic Diseases and Therapy. *Front Physiol*, **11**: 949.

Ubaida-Mohien C, Lyashkov A, Gonzalez-Freire M, et al. 2019. Discovery proteomics

in aging human skeletal muscle finds change in spliceosome, immunity, proteostasis and mitochondria. *Elife*, **8**.

Varland S, Silva RD, Kjosås I, et al. 2023. N-terminal acetylation shields proteins from degradation and promotes age-dependent motility and longevity. *Nat Commun*, **14**(1): 6774.

Wang Q, Lan X, Ke H, et al. 2024. Histone β-hydroxybutyrylation is critical in reversal of sarcopenia. *Aging Cell*, **23**(11): e14284.

Wei L, Gregorich ZR, Lin Z, et al. 2018. Novel Sarcopenia-related Alterations in Sarcomeric Protein Post-translational Modifications (PTMs) in Skeletal Muscles Identified by Top-down Proteomics. *Mol Cell Proteomics*, **17**(1): 134-145.

Wu X, Xu M, Geng M, et al. 2023. Targeting protein modifications in metabolic diseases: molecular mechanisms and targeted therapies. *Signal Transduct Target Ther*, **8**(1): 220.

Xiong Y & Guan KL. 2012. Mechanistic insights into the regulation of metabolic enzymes by acetylation. *J Cell Biol*, **198**(2): 155-164.

Yang J, Chen Z, Hu W, et al. 2025. Acetylation-dependent USP7-TRIM25 axis drives oncogenic progression in non-small cell lung cancer. *Cell Death Dis*, **16**(1): 695.

Yoshihara T, Machida S, Tsuzuki T, et al. 2019. Age-related changes in histone modification in rat gastrocnemius muscle. *Exp Gerontol*, **125**: 110658.

Yu G, Wang LG, Han Y, He QY. 2012. clusterProfiler: an R package for comparing biological themes among gene clusters. *Omics*, **16**(5): 284-287.

Zhong Q, Xiao X, Qiu Y, et al. 2023a. Protein posttranslational modifications in health and diseases: Functions, regulatory mechanisms, and therapeutic implications. *MedComm (2020)*, **4**(3): e261.

Zhong Q, Zheng K, Li W, et al. 2023b. Post-translational regulation of muscle growth, muscle aging and sarcopenia. *J Cachexia Sarcopenia Muscle*, **14**(3): 1212-1227.

Zhou Y, Zhou B, Pache L, et al. 2019. Metascape provides a biologist-oriented resource for the analysis of systems-level datasets. *Nat Commun*, **10**(1): 1523.

Data Availability

The mass spectrometry proteomics data have been deposited in the ProteomeXchange Consortium (https://proteomecentral.proteomexchange.org) via the iProX partner repository with the dataset identifier IPX0014980000 (URL: https://www.iprox.cn/page/MSV022.html).

Author contributions

Q.Q.W., X.Q.L., and Y.X. designed the study. J.L, X.Q.L., C.F.G., X.W., D.Q.Z., and L.Z. analyzed the data. C.P.H. performed the experiments. J.L., X.Q.L., and C.F.G. wrote the manuscript. Q.Q.W., X.Q.L., X.L.T., and Y.X. revised the manuscript. All authors read and approved the final manuscript.

Funding

This work was supported by the National Key R&D Program, Ministry of Science and Technology of China (2023YFC3603300, 2023YFF1001000), the National Natural Science Foundation of China (82471591, 82460283, 82560284), the Start-up Fund for Doctoral Research at the Affiliated Hospital of Guizhou Medical University (gyfybsky-2022-38), Guizhou Province (Qiankehebasis-ZK [2024] general 241), the 2025 Annual Hospital-Level Scientific Research Fund of Guizhou Hospital of Beijing Jishuitan Hospital (JGYYK[2025]-24) and the Key Medical Discipline Construction Project of Guizhou Provincial Health Commission during 2025-2026.

Conflicts of interest

The authors declare that there are no conflicts to declare.

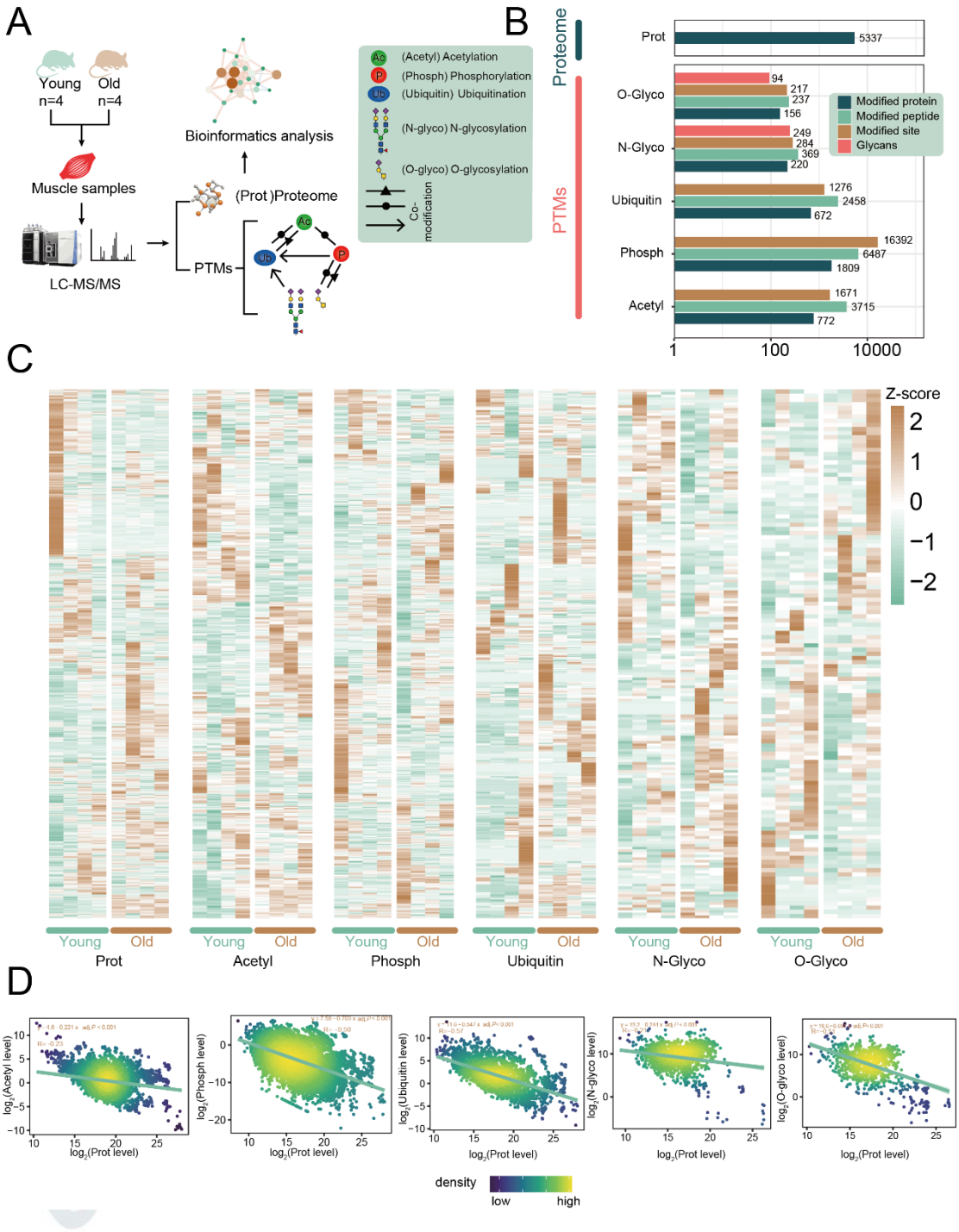

Figure 1. Integrated proteomic and PTM-omic profiling of young and aged skeletal muscle. (A) Schematic overview of the experimental and analytical workflow. Quadriceps muscles were collected from young (3-month-old) and aged (24-month-old) mice (n = 4 biological replicates per group). Muscle samples were subjected to global proteome analysis and PTM-specific enrichment for acetylation, phosphorylation, ubiquitination, N-glycosylation, and O-glycosylation, followed by LC–MS/MS

acquisition and integrative bioinformatic analysis. **(B)** Bar plots summarizing dataset coverage for the global proteome and each PTM layer. Shown are the numbers of identified modified proteins, modified peptides, modification sites, and (for glycosylation datasets) glycans detected in each analysis. **(C)** Heatmaps showing Z-score–normalized abundance profiles of the global proteome and each PTM dataset (acetylation, phosphorylation, ubiquitination, N-glycosylation, and O-glycosylation) in young and aged skeletal muscle samples. Each row represents a protein or modification site, and each column represents an individual biological replicate. **(D)** Density scatter plots illustrating the relationship between protein abundance and PTM levels across the proteome. For each PTM type, $\log_2$-transformed PTM intensities are plotted against $\log_2$-transformed protein abundances. Points are colored by local density.

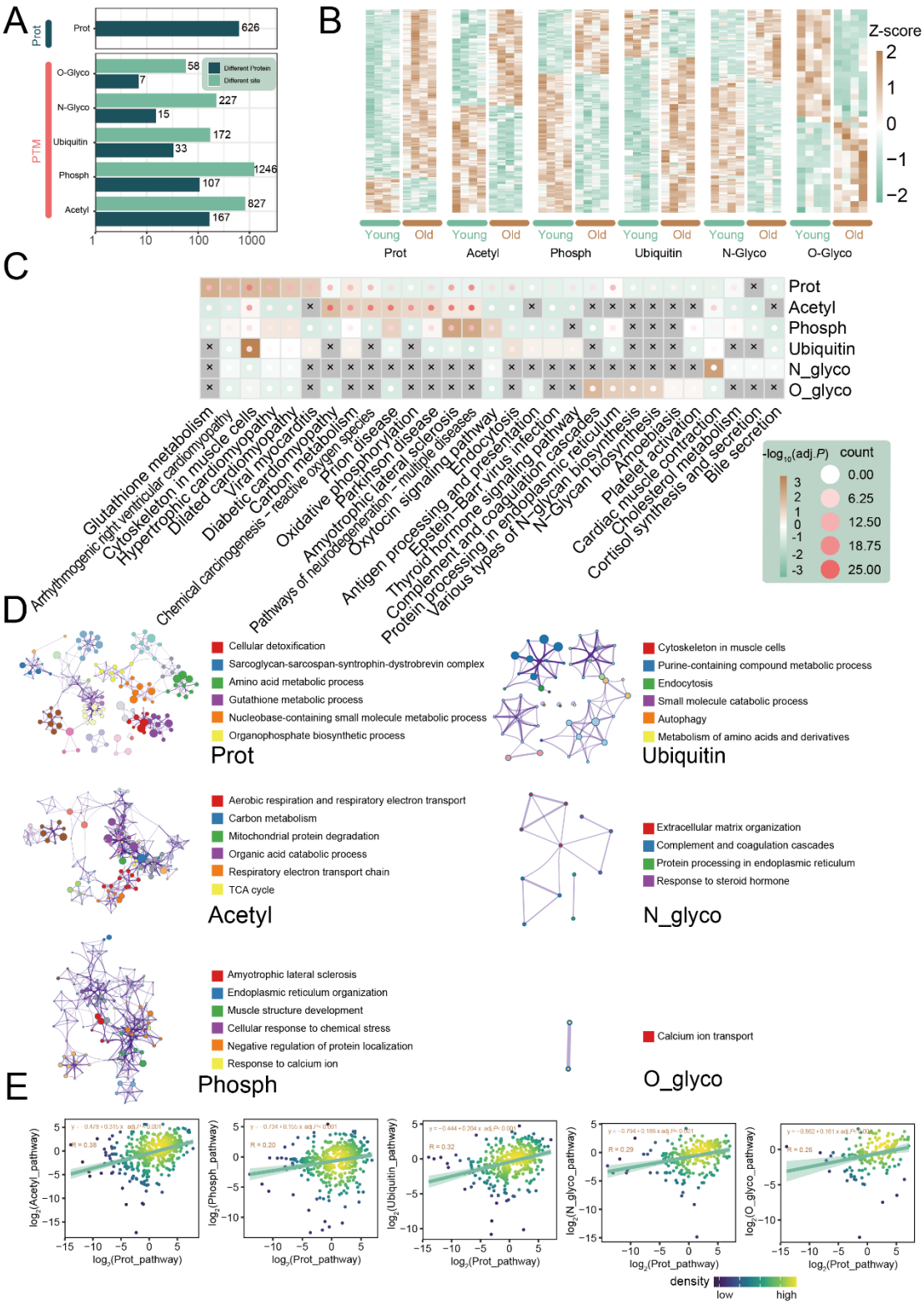

Figure 2. Global alterations in the proteome and PTM-ome of aged skeletal muscle.

(A) Bar plot summarizing the number of significantly altered proteins and modification sites identified in young versus aged skeletal muscle across the global proteome and individual PTM datasets, including acetylation, phosphorylation, ubiquitination, N-

glycosylation, and O-glycosylation. Differential changes were defined using the criteria $P < 0.05$ and $|\log_2 \text{fold change}| > 0.26$. Bars distinguish proteins exhibiting changes in abundance from modification sites showing altered PTM levels. **(B)** Heatmaps illustrating relative abundance or modification-level changes between young and aged muscle samples for the proteome and each PTM dataset. Values are Z-score–normalized within each dataset to highlight age-associated expression patterns. **(C)** KEGG pathway enrichment heatmap for significantly altered proteins and PTM sites. Color intensity of the grid represents enrichment significance expressed as $-\log_{10}$ (adjusted *P* value), while dot intensity indicates the number of proteins or modification sites contributing to each enriched pathway. Black crosses denote pathways that did not reach statistical significance after multiple-testing correction. **(D)** Functional enrichment networks of GO biological process terms for the proteome and individual PTM datasets. Nodes represent significantly enriched GO terms, and edges indicate functional similarity based on shared genes. Node colors denote major functional categories, highlighting dataset-specific and shared biological processes associated with skeletal muscle aging. **(E)** Density scatter plots comparing KEGG pathway activity scores between the global proteome and each PTM layer. Each dot represents one KEGG pathway. Axes show $\log_2$-transformed pathway activity scores, with points colored by local density.

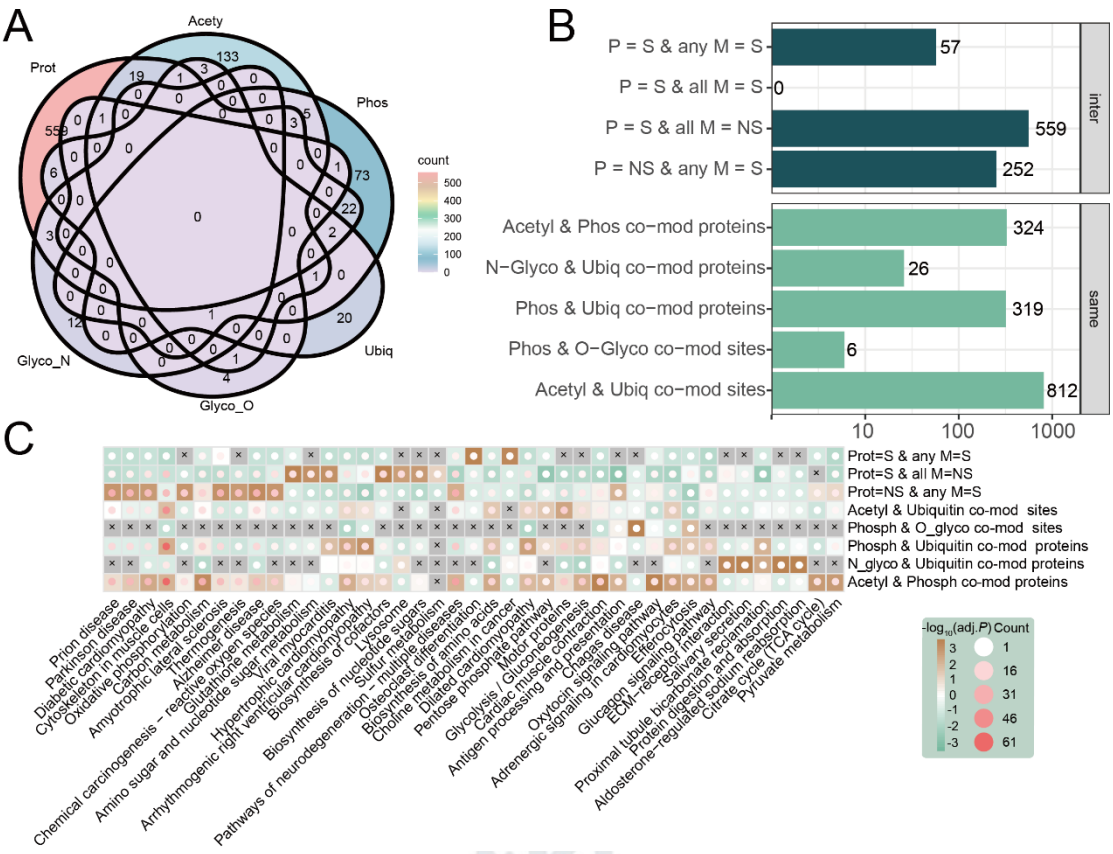

Figure 3. PTM-associated network in skeletal muscle aging. (A) Venn diagram illustrating the overlap between proteins significantly altered at the global proteome level and proteins exhibiting significant changes in one or more PTM layers, including phosphorylation, acetylation, ubiquitination, N-glycosylation, and O-glycosylation. Numbers indicate the counts of proteins shared between different datasets. **(B)** Bar plot summarizing protein and site categories based on differential regulation across the proteome and PTM datasets. Upper panels classify proteins according to their regulation status: Prot = S & any M = S, proteins significantly altered at the proteome level and in at least one PTM layer; Prot = S & all M = NS, proteins significantly altered at the proteome level but without significant changes in any PTM dataset; and Prot = NS & any M = S, proteins with unchanged global abundance but significant alterations in at least one PTM layer. Lower panels summarize PTM co-occurrence patterns at the protein or site level, including proteins modified by both acetylation and phosphorylation, phosphorylation and ubiquitination, or N-glycosylation and ubiquitination, as well as site-level co-detection of phosphorylation and O-

glycosylation or lysine residues detected with either acetylation or ubiquitination. **(C)** KEGG pathway enrichment heatmap for protein or modification-site subsets defined in panel B. Color intensity of the grid represents enrichment significance expressed as $-\log_{10}$ (adjusted *P* value), and dot intensity indicates the number of proteins or sites associated with each pathway. Black crosses denote pathways that did not reach statistical significance after multiple-testing correction. Enrichment patterns highlight distinct biological processes preferentially associated with proteome-level regulation, PTM-level regulation, or specific PTM co-occurrence categories during skeletal muscle aging.

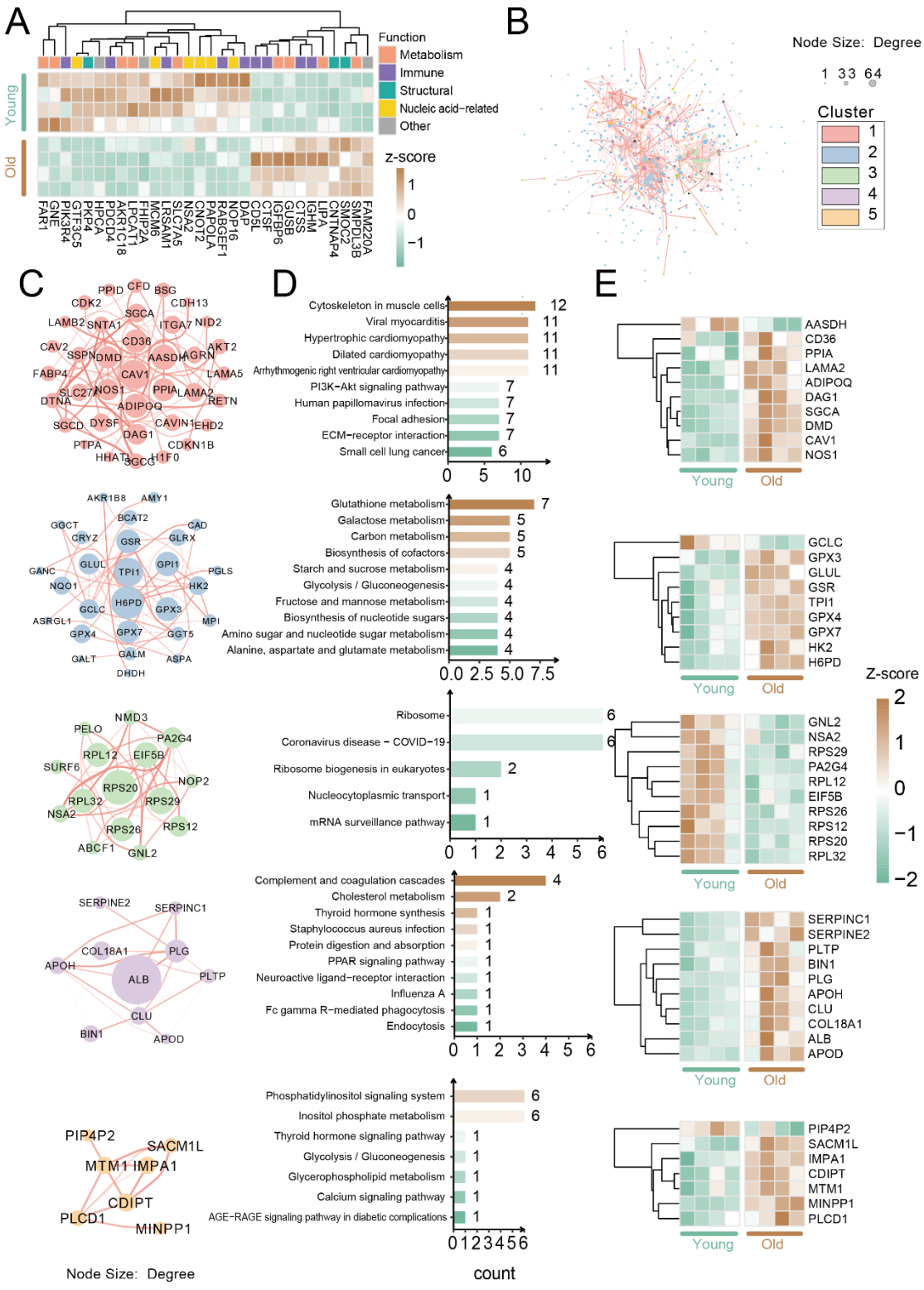

Figure 4. Proteome-level network remodeling and functional module organization in aging skeletal muscle. (A) Heatmap showing Z-score–normalized expression patterns of the top 30 differentially expressed proteins between young and aged skeletal muscle samples. Columns represent individual biological replicates, and rows represent

proteins. Functional annotations (metabolism, immune, structural, nucleic acid–related, and others) are indicated by the color bar at the top. **(B)** PPI network constructed from significantly altered proteins using the STRING database. Nodes represent proteins and edges indicate known or predicted interactions. Node size reflects degree centrality, and node color denotes cluster membership identified by DBSCAN clustering (Clusters 1–5). **(C)** Subnetwork visualization of the five major functional clusters identified in panel B. Each subnetwork highlights proteins within a given cluster and their intra-cluster interaction structure. **(D)** KEGG pathway enrichment analysis for proteins within each cluster. Bar length indicates the number of proteins associated with each enriched pathway, and color intensity represents enrichment significance ($-\log_{10} P$ value). **(E)** Heatmaps showing Z-score–normalized expression patterns of highly connected proteins (hub proteins) within each cluster, selected based on degree centrality. Expression levels are shown for young and aged skeletal muscle samples.

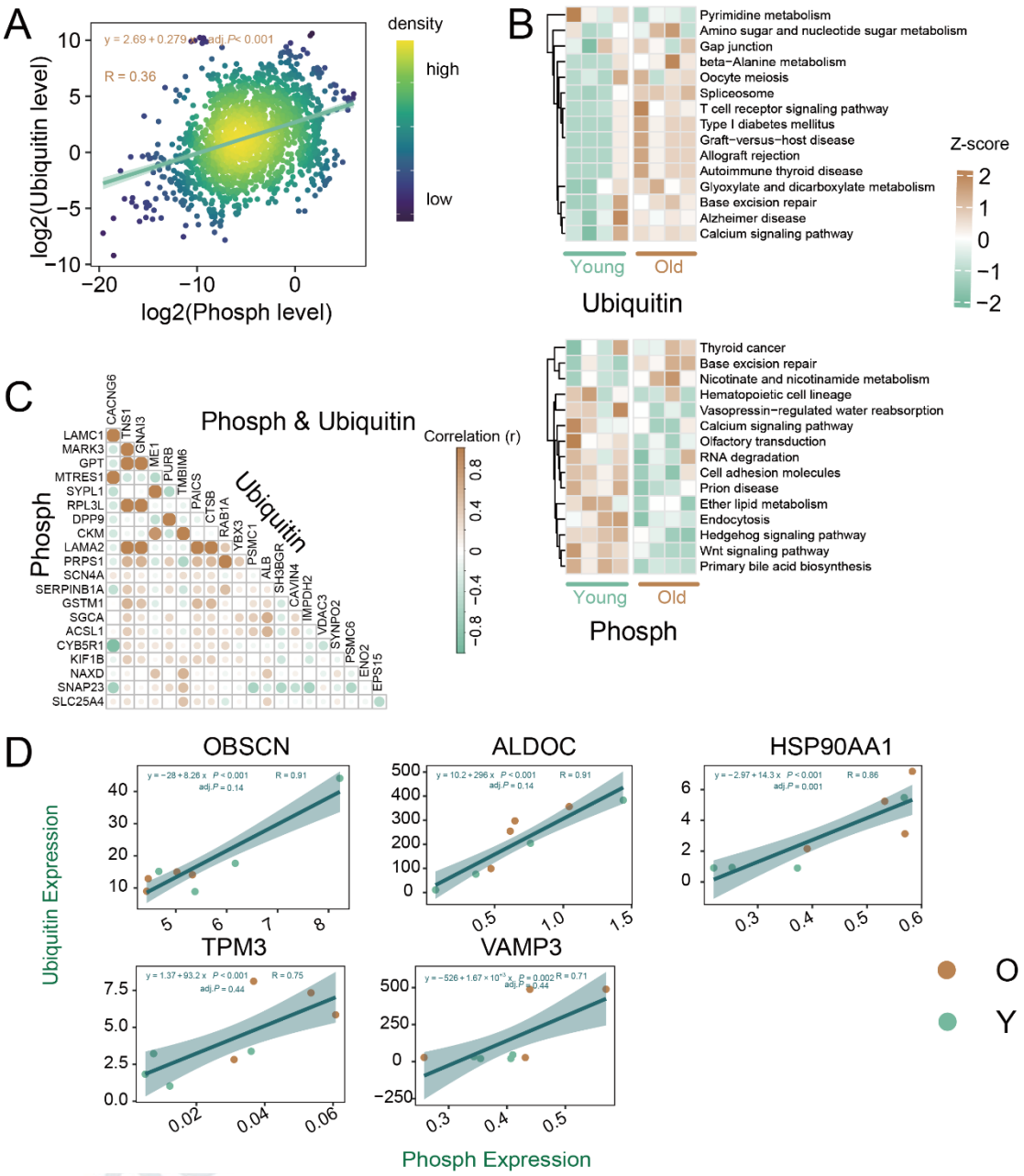

Figure 5. Association patterns between phosphorylation and ubiquitination during skeletal muscle aging. (A) Density scatter plot showing the proteome-wide association between phosphorylation and ubiquitination levels across skeletal muscle proteins. Each dot represents one protein, with phosphorylation and ubiquitination intensities plotted as $\log_2$-transformed values. Point color indicates local point density. **(B)** Heatmaps showing Z-score–normalized KEGG pathway modification scores for ubiquitination (upper panel) and phosphorylation (lower panel) in young and aged skeletal muscle samples. **(C)** Protein-level correlation heatmap illustrating Pearson

correlation coefficients (r) between phosphorylation and ubiquitination across proteins detected with both modifications. Color scale represents correlation strength. **(D)** Representative scatter plots showing protein-level associations between phosphorylation and ubiquitination for selected proteins. Each dot represents one biological replicate (young or aged), phosphorylation and ubiquitination intensities are shown.

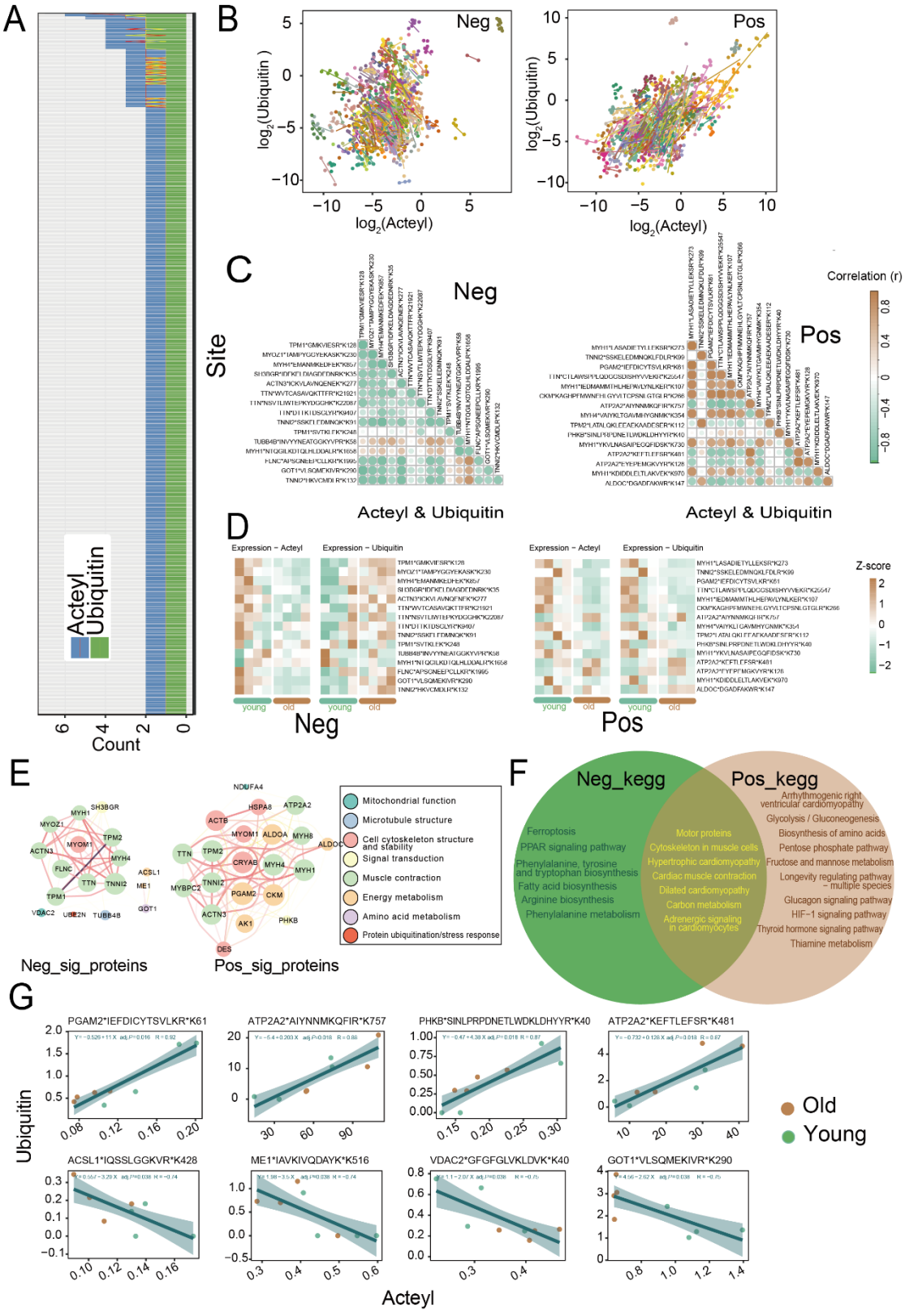

Figure 6. Site-specific association patterns between lysine acetylation and ubiquitination in aging skeletal muscle. (A) Stacked bar chart showing the distribution of lysine residues modified by acetylation only, ubiquitination only, or both

modifications across the skeletal muscle proteome. Bars indicate the number of modified lysine sites detected for each category. **(B)** Site-level scatter plots depicting the relationship between acetylation and ubiquitination intensities across lysine sites detected with both modifications. Intensities are shown as log_2-transformed normalized values. Sites are separated into negative (Neg) and positive (Pos) correlation groups based on the direction of Pearson correlation coefficients. **(C)** Correlation heatmaps showing the top 15 lysine sites with the strongest negative (left) or positive (right) correlations between acetylation and ubiquitination. Circle color represents Pearson correlation coefficients (r). Lysine sites are annotated by protein name and residue position. **(D)** Heatmaps comparing relative acetylation and ubiquitination levels of representative lysine sites between young and aged skeletal muscle samples. Values are displayed as Z-scores, calculated by row-wise standardization across all samples, where warmer and cooler colors indicate higher and lower relative modification levels, respectively. **(E)** PPI networks constructed from proteins containing highly correlated lysine sites. Nodes represent proteins, edges indicate known or predicted interactions, and node colors denote major functional categories as indicated in the legend. **(F)** KEGG pathway enrichment summary for proteins from the negative and positive correlation groups. Both shared and group-specific pathway associations are shown. **(G)** Scatter plots illustrating representative site-specific associations between acetylation and ubiquitination intensities at individual lysine residues. Each dot represents one biological replicate (young or aged).

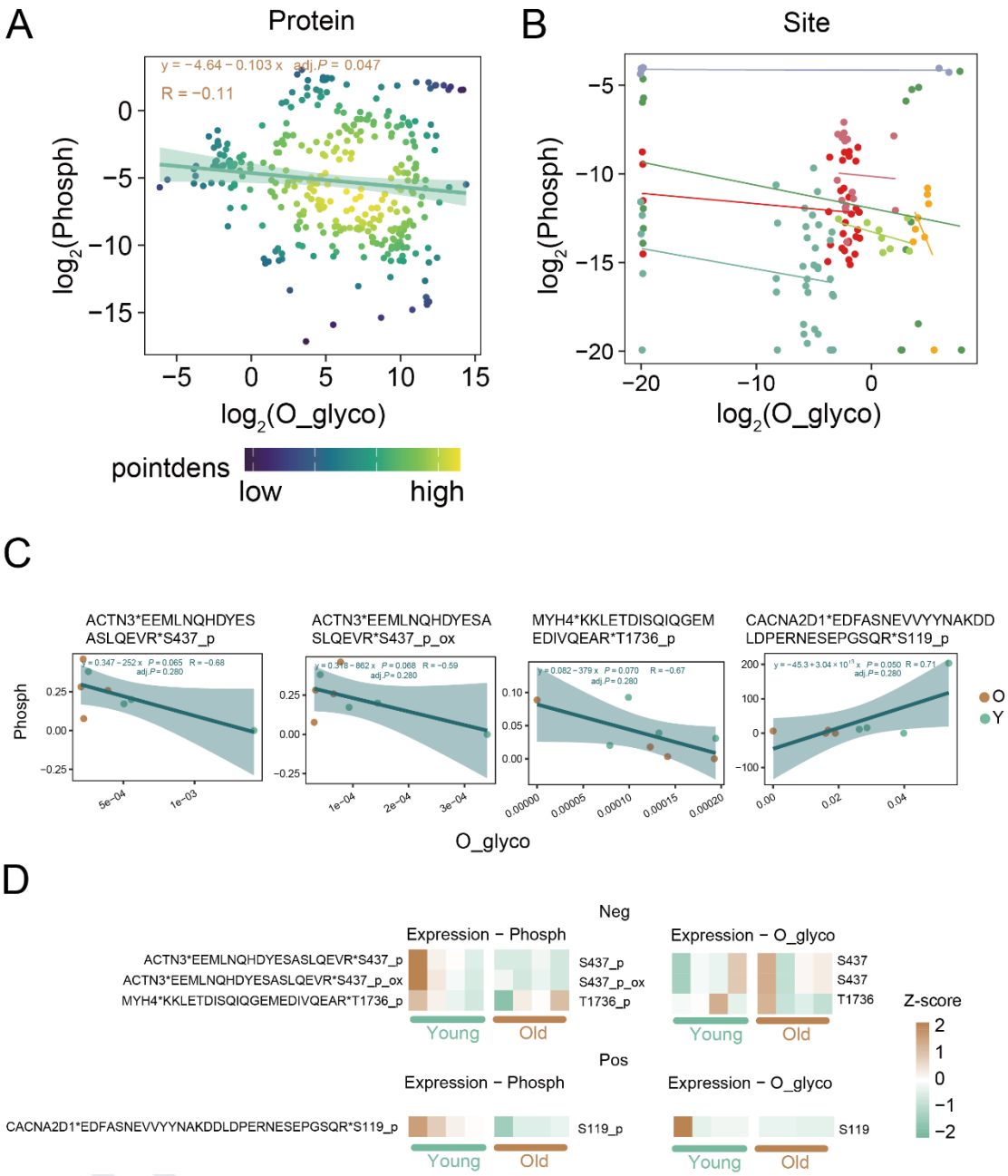

Figure 7. Association patterns between O-glycosylation and phosphorylation in aging skeletal muscle. (A) Density scatter plot illustrating the relationship between protein-level O-glycosylation and phosphorylation, where each point represents one protein. O-glycosylation and phosphorylation intensities are shown as $\log_2$-transformed normalized values. Point color indicates local point density. **(B)** Site-level scatter plot from a representative protein, showing heterogeneous associations between phosphorylation and O-glycosylation across individual modification sites. Each dot represents a distinct modification site, plotted using $\log_2$-transformed site intensities.

Colored lines denote linear regression fits for different correlation groups. **(C)** Representative examples of site-specific correlations between phosphorylation and O-glycosylation intensities. Each dot represents one biological replicate (young or aged). **(D)** Heatmaps showing relative phosphorylation and O-glycosylation levels of selected correlated sites on ACTN3 and CACNA2D1 in young and aged skeletal muscle samples. Values are displayed as Z-scores, calculated by row-wise standardization across all samples, where warmer and cooler colors indicate higher and lower relative modification levels, respectively.

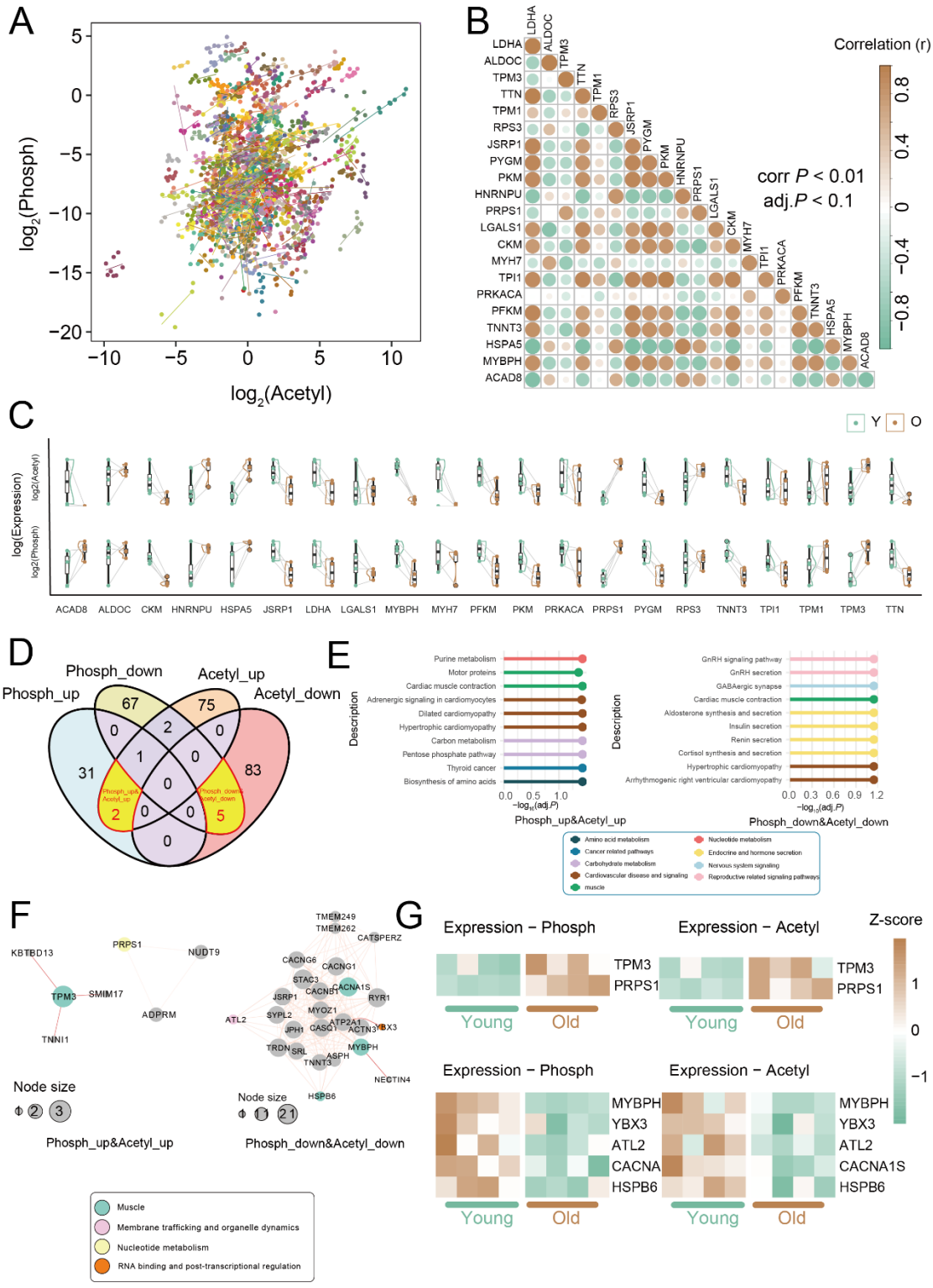

Figure 8. Association patterns between acetylation and phosphorylation in aging skeletal muscle. (A) Protein-level scatter plot showing the relationship between acetylation and phosphorylation intensities across proteins detected with both modifications. Each point represents one protein, plotted using log₂-transformed

normalized acetylation and phosphorylation intensities. **(B)** Correlation matrix of proteins exhibiting statistically significant associations between acetylation and phosphorylation. Circle color represents Pearson correlation coefficients (r). **(C)** Boxplots illustrating age-associated differences in acetylation and phosphorylation levels for representative proteins in young and aged skeletal muscle samples. Values represent $\log_2$-transformed normalized intensities. Each point corresponds to an individual biological replicate. **(D)** Venn diagram summarizing proteins exhibiting coordinated changes in acetylation and phosphorylation in aged muscle, including concurrent increases (acetyl_up & phosph_up) or concurrent decreases (acetyl_down & phosph_down). Numbers indicate the count of proteins in each category. **(E)** KEGG pathway enrichment analysis of proteins showing coordinated increases or decreases in acetylation and phosphorylation. Lollipop length represents $-\log_{10}(P)$ values, and dot colors denote major functional categories. **(F)** PPI networks constructed from proteins exhibiting concurrent increases or decreases in acetylation and phosphorylation. Node size reflects protein connectivity (degree), and node color indicates functional classification. **(G)** Heatmaps showing relative acetylation and phosphorylation levels of selected proteins with coordinated modification changes in young and aged skeletal muscle samples. Values are displayed as Z-scores, calculated by row-wise standardization across all samples, where warmer and cooler colors indicate higher and lower relative modification levels, respectively.